Characterisation of polymeric network structures

Peters, R.

7 Characterisation of UV-cured acrylate networks as studied by thermal degradation methods

Abstract

UV-cured mixtures of bi-functional polyethylene glycol di-acrylate and mono-functional 2-ethylhexyl acrylate were analysed by different thermal degradation methods, to investigate the feasibility of these methods.
Thermogravimetric analysis (TGA) and differential scanning calorimetry (DSC) give insight in the thermal decomposition temperature, while pyrolysis-electron ionisation mass spectrometry (Pyr-EI-MS) shows different series which reflect the polyethylene glycol chains between network junctions and the acrylate backbone chains. The use of pyrolysis-chemical ionisation mass spectrometry (Pyr-CI-MS) shows the release of similar series, however less fragmentation upon thermal degradation occurred. A 'solid' sample preparation technique and matrix-assisted laser desorption ionisation was used to form ions from the network surface followed by time-of-flight mass spectrometry (MALDI-TOF-MS). To increase the reliability of the MS-data interpretation, liquid chromatography mass spectrometry (LC-MS) analysis upon pyrolysis was performed. Off-line Pyr-LC-MS shows different series reflecting the acrylate network structure. The same result was observed using the designed on-line-Pyr-LC-MS analysis. However, peak broading of low-molecular-weight polar compounds, as a result of the used dissolution/injection procedure was observed.
In conclusion, the use of thermal degradation methods followed by MS or LC-MS analysis results in thermal degradation products of cross-linked acrylates which confirm the acrylate network structure and give insight in the chemical composition. However, no indication of network imperfections was observed. Thermal degradation temperatures, as observed by TGA, DSC or Pyr-MS, show a linear increase with the network density.

7.1. Introduction

UV-cured acrylates are mostly dense networks, which have a broad industrial application field such as paints, adhesives and optical fibres. UV-curing of acrylates offers several advantages, such as fast curing, reduced emission (solvent free) and simplicity of application [1].
The general formulation of solvent free acrylate coatings is a reactive acrylate resin and a reactive acrylate diluent (1-50%). Both the acrylate resin (oligomer) the acrylate diluent can be multi-functional. The role of the diluent is to adjust the viscosity of the mixture to an acceptable level for application, but its most important function is to adjust the final cross-link density. The acrylates have a chemical structure which can be varied and can consist of polyethers, polyesters, aliphatic and aromatic urethanes, carbonates or other types of oligomers [1,2]. A typical example of a cross-linked acrylate polymer is a photo-cured mixture of bi-functional polyethylene glycol di-acrylate (PEGDA) and mono-functional 2-ethylhexyl acrylate (EHA)(see *Fig.* 7.1).

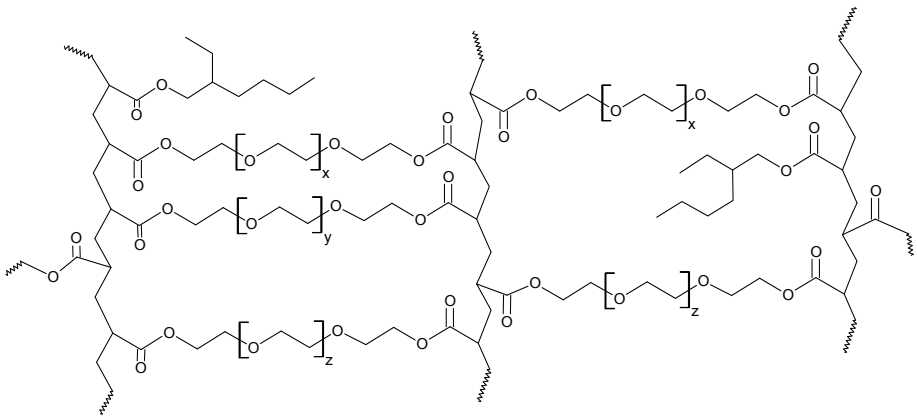

Fig. 7.1. Schematic representation of UV-cured PEGDA/EHA acrylate network.

These cross-linked acrylate polymers are generally characterised by their physical and mechanical properties, such as the glossy body, sag resistance, high mechanical strength and resistance to water, oil and alcohol as well as to many other chemicals [1]. These properties are largely influenced by the mean molecular weight of viscoelastic chains between network junctions, chemical composition, acrylate conversion and network structure (type of network junctions, network imperfections and heterogeneity). To improve the performance of these UV-curable acrylates, it is required to elucidate the

chemical structures of the cured networks and related them to their mechanical and physical properties.

Different techniques have been applied to study these acrylate networks. Their photo-polymerisation kinetics have been investigated using real-time infrared spectroscopy [3–5] and differential scanning calorimetry [6,7], while the heterogeneity, cross-link density and spatial distribution of cross-links have been studied using solid-state nuclear-magnetic resonance (s-NMR) spectroscopy [8,9]. These techniques give valuable information, however, they do not allow the complete chemical characterisation of the network structures.

To gain more insight in the network structures, chemical degradation is often used as a sample preparation method, followed by chromatographic and mass spectrometric analysis [10–13]. The concentration and the molecular weight distribution of the kinetic chain and chains between cross-link junctions are typically results obtained using this kind of indirect analysis of these non-soluble cross-linked acrylates.

Another way of indirect analysis is the use of thermal degradation methods, followed by analysis of the degradation products. Thermal degradation, often called pyrolysis, is the chemical transformation induced by thermal energy alone when a compound is heated at a temperature significantly higher than ambient. The main effect of pyrolysis is typically the decomposition of the initial compounds with formation of smaller molecules [14]. If the degradation is followed by determination of average macroscopic changes, such as the weight or other physical or mechanical properties it is called thermal analysis. This includes thermogravimetric analysis (TGA), differential thermal analysis (DTA), differential scanning calorimetry (DSC) and thermo-mechanical analysis (TMA)[15]. The use of these techniques gives information about physical properties, such as glass-transition temperature (T_g), melting point, thermal stability and flammability. Pyrolysis is commonly followed by gas chromatographic- mass spectrometric analysis (Pyr-GC-MS). However, other combinations of pyrolysis and analysis are known, such as pyrolysis-infrared spectroscopy or in-source pyrolysis-mass spectrometry (Pyr-MS) [16].

Pyrolysis, followed by analysis of the degradation products, is an important technique for the composition determination in polymer characterization [14,16,17]. The thermal degradation fragments often contain sufficient information to identify the chemistry of the original polymer; however, information about the average molecular weight will often be lost. A classic example of Pyr-GC-MS is the determination of the monomeric composition of ethylene/propylene copolymer [18]. Another application of Pyr-GC-MS is the determination of the number average sequence length of various non-cross-

linked copolymers, such as styrene-butyl acrylate, chlorinated polyethylene, styrene-methyl methacrylate, vinyl-chloride-vinylidene-chloride and styrene-maleic anhydride copolymers [19].

The use of pyrolysis for the characterisation of cross-linked polymers is rather limited. Pyr-GC-MS has been utilised for the characterisation of vulcanised rubbers [20], polystyrene gels [21] and cross-linked polyesters [22,23]. Matsubara *et al.* described the characterisation of an UV-cured acrylate network in terms of chain-length distribution of network chains using Pyr-GC-MS [24]. The authors suggested that the chain-length distribution of the repeating acryloyl groups could be determined from their results. However the low recovery of acrylate polymer in GC due to their low volatility and the possible C-C cleavage make the determination of the chain-length distribution unreliable. In the case of oligomeric or polar degradation compounds, liquid chromatography instead of gas chromatography can be used upon pyrolysis. This was demonstrated by Van der Hage *et al.*, who used pyrolysis, coupled to LC-MS for the analysis of collagen-based materials [25].

Although limited characterisation studies of acrylate networks by pyrolysis are described, extensive studies are performed of the degradation of non-cross-linked polymers. Since acrylate networks of PEGDA can be represented as polyacrylate backbone chains and polyethylene glycol (PEG) chains between network junctions, the described degradation mechanism of both non-cross-linked polyacrylate and PEG polymers was reviewed.

In general, the degradation mechanisms experienced by polymers are free-radical processes initiated by bond dissociation at the pyrolysis temperature. It should be emphasized that degradation itself is a complex multi-stage process. It consists of a series of consecutive and simultaneous reactions of initiation, depolymerisation, scission of the side and of the main chains, chain termination and recombination, each with its own kinetic parameters. Moreover, each specific process has its own individual mechanism depending on experimental conditions, such as temperature, heating rate, atmosphere, sample size, sample composition *etc.*

The thermal degradation of poly-*n*-alkyl acrylates was systematically studied by Bertine *et al.*, who found two main degradation mechanisms which include random main-chain scission and side-chain reactions [26]. Cameron and Kane [27] suggested that the initial radicals abstract tertiary hydrogen atoms from the main chain, resulting in the formation of a resonance-stabilised radical, which initiates the depolymerisation of the main backbone chain. Unzipping (also called depropagation or depolymerisation) of the main chains gives very high yields of monomers [28]. Besides monomers, significant concentrations of

dimers, saturated dimers and even trimers are observed as a result of pyrolysis (*Fig.* 7.2). The scission takes place under conditions of thermodynamic control; the quantitative yield depends on the stability of the radicals and compounds formed. The intramolecular transfer is followed by chain scissions, with a significantly higher yield of trimers compared to dimers, as the six-member ring formation is thermodynamically most stable in systems with carbon-carbon bonds. This makes the quantitative result not consistent with a random scission mechanism [29]. Mahalik *et al.* show that the main-chain scission decreases with an increase in the alkyl chain length of poly-*n*-alkyl acrylates [30]. Similar depolymerisation reactions are found for poly-*n*-alkyl methacrylates [26,31], poly(diethyl fumarate) [32] and fluorinated alkyl (meth)acrylate [33].

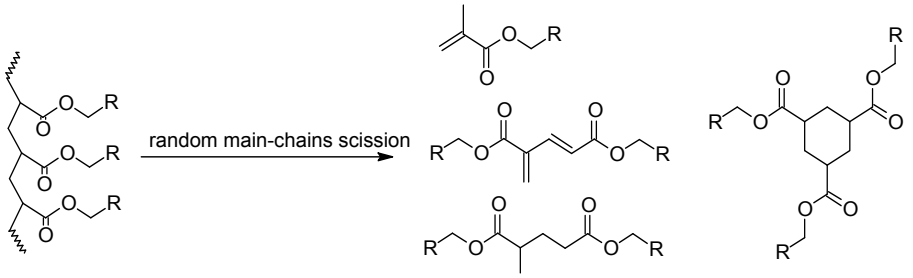

Fig. 7.2. Random main-chain scission of alkyl-n-polyacrylates.

The second thermal degradation pathway of poly-*n*-alkyl acrylates are the non-radical side-chain reactions towards alkenes, alcohols and trace amounts of aldehydes degradation products (*Fig.* 7.3a, b, c). The formation of an alkene can occur via direct release of the alkane, followed by decarboxylation of the acid group [34]. However, IR analysis shows that there may be some tendency for alkane release to occur unaccompanied by CO_2 production, which indicates that the formation of alkane occurs by the reaction of the β-hydrogen atoms to the carbonyl group via a six-member transition state [34]. The anhydride moieties (see *Fig.* 7.3d) could be formed in the polymer chain by loss of water or an alcohol [35]. The concentration of the two main pyrolysis products, alkenes and alcohols, is independent of the alkyl chain length (n= 2-12). The formation of the alcohol shows a strong decrease with the pyrolysis temperature as result of the accelerated decarboxylation at higher temperatures [26,34]. Direct pyrolysis of model compound palmityl acrylate shows the formation of acrylic acid and hexadecane (dealkylation) [36]. With alkyl acrylate esters, the ester decomposition becomes possible when the monomer unit incorporates at least one β-hydrogen atom (*e.g.* poly *i*-propylacrylate or poly *t*-butylacrylate) [37].

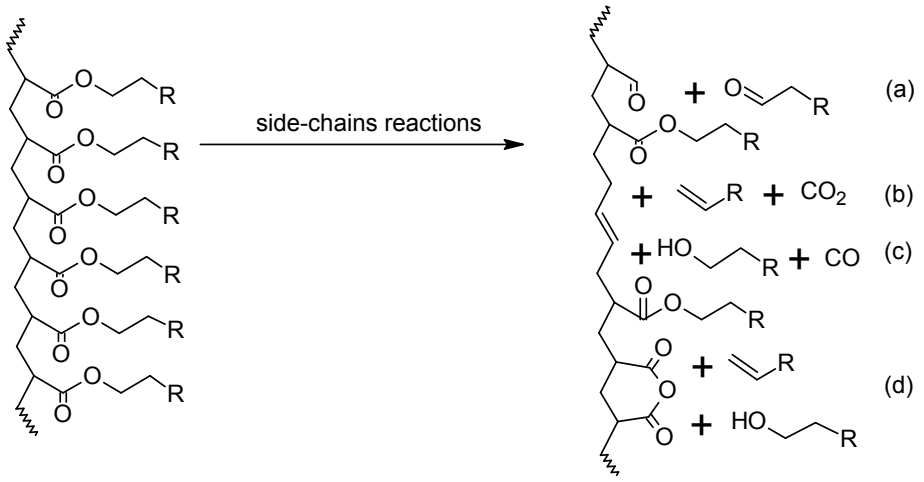

Fig. 7.3. Side-chain reactions of alkyl-n-polyacrylates.

Thermal degradation of PEG (see *Fig.* 7.4) shows the preferred cleavage of C-O bonds at the onset of pyrolysis; H-abstraction following C-O homolysis produces hydroxyl and 'ethyl-ether' endgroups [38]. At higher temperatures, the abundances of the 'methyl-ether' and 'ethyl-ether' endgroups become more balanced as relatively more C-C cleavage occurs, combined with cleavage of formaldehyde [39]. The increasing abundance of 'vinyl-ether' endgroups at higher pyrolysis temperatures is primarily due to dehydration of hydroxyl endgroups [40].

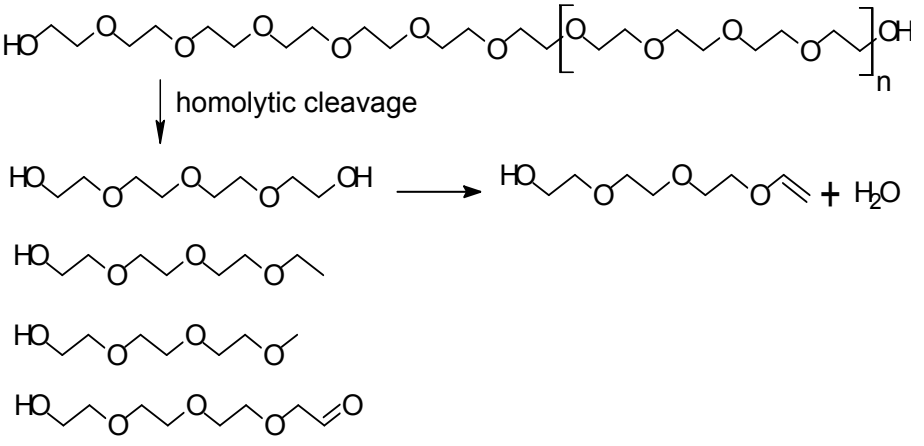

Fig. 7.4. Thermal degradation routes of PEG.

Pyrolysis of PEG endcapped with acrylate or methacrylate, show similar fragments, as are observed from pyrolysis of PEG alone [40]. The endgroups, alone or connected with fragments of ethylene glycol oligomer, were also observed in the pyrolysate. Although matrix-assisted laser desorption ionisation followed by time-of-flight-mass spectrometry (MALDI-TOF-MS) is considered to be a soft ionisation technique, pyrolysis upon ionisation by MALDI was obtained for PEG [41]. Both 'methyl-ether' and 'vinyl-ether' endgroups are observed. Degradation of PEG in air (80°C at 1000 h) followed the chain scission mechanism for oxidative degradation, resulting in low-molecular-weight esters [42].

In this chapter, thermal degradation methods for the characterisation of highly cross-linked non-soluble PEGDA/EHA networks, with different ratios of mono- and bi-functional acrylates, are investigated. The goal is to use various thermal degradation methods, followed by different analysis techniques, in order to review the possibilities of these thermal degradation methods for the characterisation of UV-cured acrylate networks.

First, DSC and TGA were used to study the thermal stability of these dense networks. Secondly, Pyr-MS was studied, where a probe with a heated filament was used to produce heat inside the MS-source to desorb molecules that are ionised by electron-ionisation (EI) or chemical-ionisation (CI). MALDI-TOF-MS, in combination with a 'solid' sample preparation method, was investigated as a direct thermal analysis method of the chemical networks. The focussing power of the laser beam of the MALDI-ion-source was used to form characteristic ions from the network surface. The MS-spectra of these direct pyrolysis-MS techniques (Pyr-MS, MALDI-TOF-MS) are complex and difficult to interpret, so additional separation of the thermal degradation fragments was used to simplify the interpretation. In the case of PEG oligomeric degradation products, GC analysis gives additional problems, such as low recoveries of the higher molecular weight products. To avoid these GC-related problems and simplify the elucidation of thermal degradation fragments, on-line pyrolysis-LC-MS was developed. The feasibility of these thermal degradation approaches for the characterisation of acrylate networks will be discussed.

7.2. Experimental

The formulations, prior to UV-curing, were prepared from mixtures of polyethylene glycol di-acrylate (PEGDA, M_n = 700 *Da*, Aldrich Chemical Company Inc., Milwaukee, USA) and 2-ethylhexyl mono-acrylate (EHA,

Aldrich Chemical Company). The UV-cured acrylate polymers were mixtures of PEGDA and 0, 20, 40 and 60% (*w/w*) EHA. The formulations contained 1% (*w/w*) of photo-initiator 1-hydroxycyclohexyl phenyl ketone (Irgacure 184, Ciba Geigy, Basel, Switzerland). The different ratios of mono- and bi-functional acrylates were used to vary the mean network density. The mixtures are designated with numbers (*i.e.* PEGDA/EHA(60:40)), which represent the concentration of the monomers in weight percent. The preparation and the characterisation of the used acrylate networks is outlined in Chapter 2 [12].

The DSC experiments were carried out using a Mettler DSC 82 instrument (Mettler-Toledo International, Inc., Tiel, The Netherlands). About 5 mg UV-cured PEGDA/EHA was placed in an open aluminium cup and purged with 80 mL nitrogen/min during the experiment. The starting temperature was 40°C, heating speed was 10°C/min and the end temperature was 500°C. Data analysis was performed with a Mettler Toledo Star System (Mettler-Toledo Int.). The TGA experiments were performed using a TGA-7 instrument (Perkin Elmer, Inc., Boston, USA), using similar heating conditions as with DSC. The data analysis was performed with Pyris software (Perkin Elmer).

The Pyr-MS experiments were performed using probe-MS (thermal desorption inside the MS-source). These experiments were performed with the use of an E/B/E sector instrument (AutoSpecE, Micromass, Manchester, UK) under standard EI (70 eV, 10^{-7} mbar) and CI conditions. Pyr-EI-MS was performed using about 1 mg of UV-cured PEGDA/EHA in a borate-silica cup (solid-probe) in high vacuum, which was heated from 50°C to 450°C with a heating rate of 10°C/min. The sample stays 5 minutes at the end-temperature of 450°C. Pyr-CI-MS was performed with ammonia as CI gas ($3*10^{-5}$ mbar). The source temperature was 150°C, the emission current was 0.5 mA and the electron energy was 40 eV. The samples were heated from 100°C to 450°C with a heating rate of 10°C/min. The sample stays 10 minutes at the end-temperature of 450°C.

MALDI-TOF-MS experiments were performed with a Micromass Tof Spec 2E (Micromass, United Kingdom) with delayed extraction. A 337 nm UV-nitrogen laser producing 38 ns pulses was used, and the MS-spectra were obtained in the reflection mode. The operating voltage was 20 kV, positive, while the MS-spectra were collected in the range from m/z = 50-5000. The mass spectral data were processed with Masslynx MALDI-TOF-MS software, version 3.0 (Micromass, 1997, United Kingdom). Cured PEGDA/EHA(80:20) was investigated with MALDI-TOF-MS, using three different sample preparation methods: unground, crude ground and fine ground films. The crude ground sample was prepared by using cryogenic grinding of the sample in the presence

of sodium chloride (NaCl) in the ratio 1:1. The mixture was ground during 10 minutes using liquid nitrogen (N_2) at -196°C with a SPEX Freeze/Mill system (SPEX Industries, Inc., NJ, USA). After grinding, the NaCl in the sample was dissolved in water and the sample (non-soluble part) was filtered (Millipore lot LC, Massachusetts, USA). The residue was washed with water en dried at room temperature using N_2. The fine ground sample was prepared using a mortar and pestle. As matrix solutions (1 mg/25 ml) combination of 2,5-dihydroxybenzoic acid (DHB, Sigma Chemical, St. Louis MO, USA) or dithranol (1,8-dihydroxy-9[10H]anthracenone, Dith, Sigma Chemical, St. Louis MO, USA) in acetonitrile (ACN, p.a. Merck, Darmstadt, Germany) or tetrahydrofuran (THF, Biosolve LTD, Valkenswaard, The Netherlands) were used. Also the addition of sodium acetate (NaAc, Merck, Germany) was investigated.

The off-line pyrolysis experiments were performed by using a temperature programmable oven: OPTIC 2 (Atas Programmable Injector, Ai Qualitek LTD, Cambridge, UK) with a standard borate-silicate liner. All the experiments were performed with one UV-cured coating; PEGDA/EHA (80:20). A few mg sample was placed into the liner above a glass-wool plug to ensure the right height for optimal heating. The starting temperature of the oven was 50°C, while the temperature ramping was 15°C/sec for all experiments. The end-temperature was varied; 250 to 400°C for a stated time. The temperature profile and weight for the different off-line pyrolysis experiments are given in Table 7.1. During the heating period, the oven was purged with a low flow of helium (oxygen free). After the heating period, the sample was cooled in a few seconds to 50°C. The thermal residues in the liner (pyrolysates) were quantitatively dissolved in 10.0 mL THF (Biosolve LTD). The dissolved fraction was analysed using liquid chromatography on a HP1100-MS system (Agilent, Waldbronn, Germany), which consisted of a degasser, quaternary pump, column oven, large volume autosampler, diode-array-detector (DAD) system with on-line a HP1100 single quadrupole MS equipped with an atmospheric pressure ionisation electrospray interface (API-ESI). Run control and data analysis was performed with ChemStation, revision A09.01 (Agilent). The separation was performed using two 250×3 mm Inertsil ODS-3 columns (Varian, Bergen op Zoom, The Netherlands) in series at 40°C. The analyses were carried out in the gradient mode using mobile phase A, which consisted of Milli-Q water (Waters, Milford, USA) and mobile phase B, which consisted of acetonitrile (ACN, p.a. Merck, Darmstadt, Germany). The gradient was started at t=0 min with 100% (*v/v*) A, stayed there for 5 min and changed then to 100% (*v/v*) B at t=45 min, where it remained constant for 15 min. The flow rate was 0.5 mL/min and the injection-volume was 5 µL. The MS-system was operated in positive mode at an

ionisation voltage of 3.5 kV, fragmentor voltage of 50 V, scan range of *m/z* 50-1500, step size 0.10 and full data storage. The eluent flow was split (1:1) by means of a zero dead volume T-piece to assure a flow of approximately 0.25 mL/min into the API-ESI interface. The interface gas and the vaporiser temperature were held constant at 350°C and the nebulizer pressure was set on 50 psi. Dry nitrogen at a flow rate of 10.0 L/min was used as nebulizer gas.

Table 7.1. The temperature profile and sample weight of the off-line Pyr-LC-MS experiments (T_{start} = 50°C, T_{ramp} = 15°C/min)

Experiment	Sample weight (mg)	T_{end} (°C)	Time at T_{end} (sec)	Total heating time (min)
1	3.89	250	46	1
2	2.20	300	43	1
3	2.48	300	283	5
4	2.52	300	883	15
5	2.88	350	280	5
6	2.62	350	880	15
7	3.08	400	37	1
8	2.11	400	277	5
9	2.60	350	40	1

The Pyr-LC-MS experiments were performed using an in-house developed Curie-Point-pyrolysis-LC-MS system. Both a direct injection and an indirect injection coupling between the pyrolyser and the LC-system were investigated. The schematic representations of both systems are given in *Fig.* 7.5. In both systems an in-house developed Curie-Point pyrolyser liner (L×ID×OD = 75×2.5×4 mm) was used, as the conventional quartz liner from Fischer (L×ID×OD = 75×3×4 mm with melted RVS-needle L = 55 mm) has some disadvantages. First, the metal-glass connection cannot stand a pressure of a few bars, which is caused by the differences in expansion coefficients of glass and metal. Secondly, the connection of the needle and the LC-system is not free from liquid- and gas leakage. The connection of the glass and the LC-system was performed by two Swagelock-nuts (1/4") with home-made PEEK-ferrules. A reducing union (1/4" to 1/16") was used to decrease the diameter to normal LC-dimensions. Using the direct injection coupling (*Fig.* 7.5a), the pyrolysis degradation products are dissolved in THF by injection of THF and trapped on top of the LC-column. The performance of this on-line CP-Pyr-LC system was investigated by using PEGDA and EHA as model compounds. Although the system works (injection of PEGDA and EHA on the LC-column), the pressure

over the pyrolyser liner, during the dissolution and injection-step, is too high (up to 40 bar), which causes breaking of the glass pyrolyser liner.

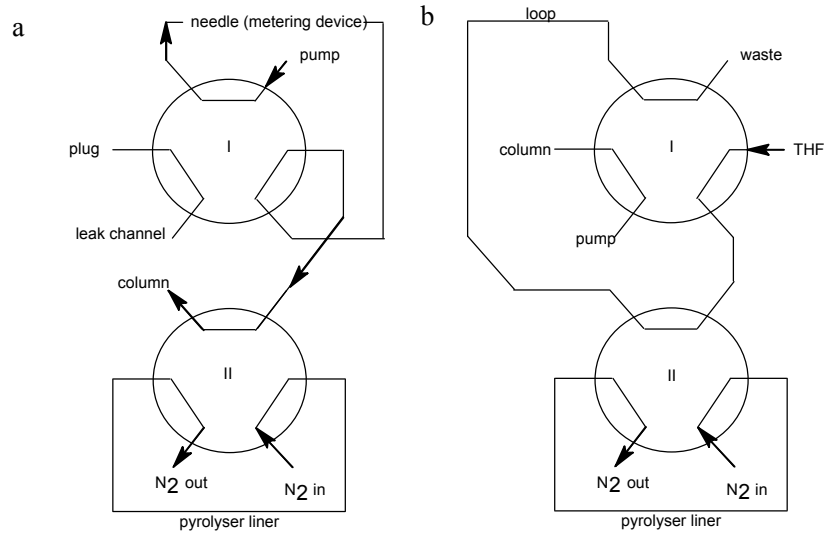

Fig. 7.5. Schematic representation of the on-line CP-Pyr-LC system with direct (a) and indirect injection procedure (b).

Therefore, the coupling between pyrolyser liner and LC-system was made with the use of a loop (500 µL sample loop, Genuine Rheodyne Products, part 70-26SL)(see *Fig.* 7.5b). The solvent (0.2 mL/min THF), to dissolve the pyrolysis products, is delivered by an external pump (Gynkotek 480 HPLC pump, Germering, Germany) in combination with a damper (125×4 mm Nucleosil 120-C18-5 column (Manchery-Nagel)) to generate a constant flow (± 30 bar backpressure). The LC and THF flow are mixed before the compounds are trapped on the LC column (2×(250×4 mm) Nucleosil 120-C18-5 (Manchery-Nagel) at RT). The compounds trapped are separated using a flow rate of 1.0 mL/min and gradient elution. The gradient starts at t=0 minutes 95% (*v/v*) A (H_2O) and 5% (*v/v*) B (ACN), t=12.5 minutes 95% (*v/v*) A and 5% (*v/v*) B, t=42.5 minutes 2% (*v/v*) A and 98% (*v/v*) B, t=45.5 minutes 2% (*v/v*) A and 98 % (*v/v*) B. To re-equilibrate the column, the initial conditions were restored at t=47.5 minutes and held for 15 minutes before the next analysis was started. The separated compounds were detected using DAD and ESI(+)-MS (HP1100-MS, Agilent). The MS-system was run in positive mode at an ionisation voltage of 3.5 kV, fragmentor voltage of 70 V, scan range of *m/z* 100-1500, step size 0.10 and full data storage. The eluent flow was split (1:4) by means of a zero dead volume T-piece to assure a flow of approximately 0.25 mL/min into the API-

ESI interface. The interface gas and the vaporiser temperature were held constant at 350°C and the nebuliser pressure was set on 50 psi. Dry nitrogen at a flow-rate of 10.0 L/min was used as nebulizer gas.
The PEGDA/EHA mixtures are directly UV-cured on the top of ferromagnetic wires (L×OD = 85×0.4 mm) using similar UV-curing conditions as described in the experimental section of Chapter 2. The pyrolysis was performed with the use of these ferromagnetic wires, which were inductively heated within 0.5 s to their Curie-point temperature with the generator (Fischer Curie Point Pyrolyzer 0316). The 1 kW generator can deliver a 10 A current at a frequency of 1.1 MHz to the high frequency coil in the pyrolysis unit. The pyrolyser liner is purged with dry N_2-gas (Chrompack-Gas Clean Oxygen filter, Varian).

7.3. Results

7.3.1. DSC and TGA of cross-linked acrylates

The thermal degradation of cross-linked acrylate networks was studied by DSC and TGA experiments. The DSC experiments show one endothermic and one exothermic peak for all the cross-linked acrylates, with different PEGDA/EHA ratios. The endothermic peak is caused by decomposition of the acrylate network. An increase in EHA concentration decreases the endothermic decomposition temperature; *i.e.* PEGDA/EHA(60:40) has a lower decomposition temperature compared to PEGDA/EHA (100:0) (Table 7.2).

Table 7.2. DSC result of different UV-cured PEGDA/EHA networks

Sample	Exothermic peak (°C)	Endothermic peak (°C)
PEGDA/EHA(40:60)	± 230	395
PEGDA/EHA(60:40)	± 230	399
PEGDA/EHA(80:20)	± 230	403
PEGDA/EHA(100:0)	± 230	407

The broad exothermic peak appears between 200 and 350°C, with a maximum at about 230°C for all these cross-linked acrylates. There are several possible explanations for this effect. First, structural changes can give a broad exothermic peak in the DSC curve. Typical examples are denaturation of egg white protein or the melting process of ill-defined crystallites in thermoplastics such as polyvinylchloride at 100-200°C. However, cross-linked acrylate is a thermoset,

which does not melt before the decomposition temperature is reached, which makes this explanation unlikely. A possibility for the exothermic peak is the glass-rubber transition of the polymer. However, the glass-transition temperature (T_g) of these UV-cured acrylates is in the order of -50°C as a result of the high cross-link density [9]. Unreacted Irgacure 184 (± 0.1%, *w/w*) can initiate cross-linking at these temperatures, while the increased mobility of unreacted monomers, will cause them to react more easily. This rest curing is likely as it will deliver energy and will give an exothermic peak.

*Table 7.3. TGA result of three different UV-cured acrylates (**low** = loss of weight)*

Sample	5 % ***low*** (°C)	50 % ***low*** (°C)	95 % ***low*** (°C)
PEGDA/EHA(40:60)	351	395	439
PEGDA/EHA(60:40)	300 (?)	403	443
PEGDA/EHA(80:20)	356	413	448
PEGDA/EHA(100:0)	359	422	452

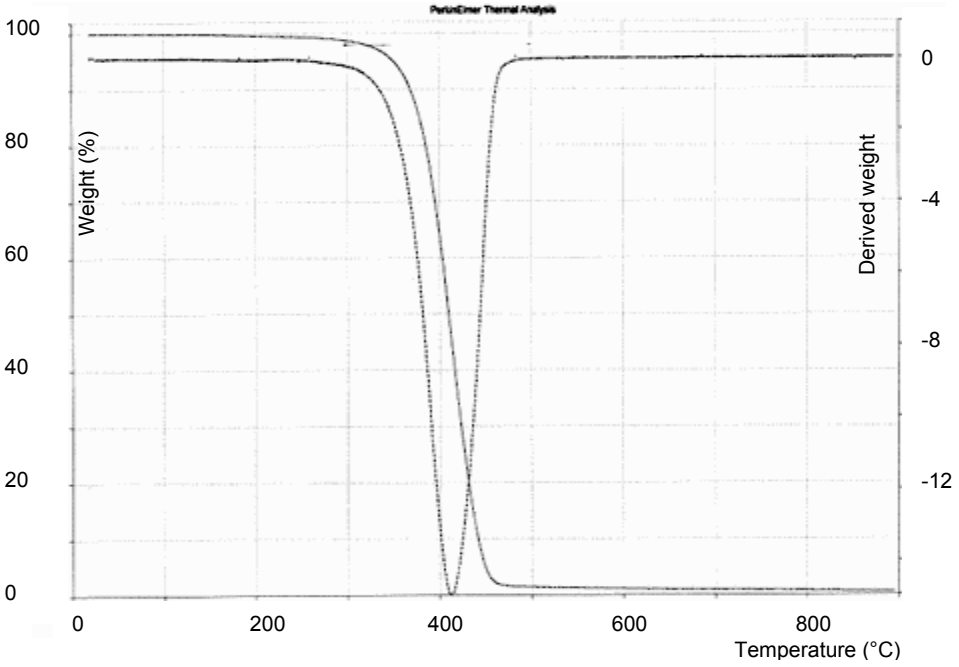

Fig. 7.6. TGA thermogram of PEGDA/EHA(80:20).

Other explanations for the broad exotherm of the acrylates are a transition in physical state of the polyester or volatilisation of monomers/oligomers from the acrylates. To investigate if volatilisation of monomers/oligomers or other small

molecules can cause the broad exotherm, TGA was used. The TGA thermogram of PEGDA/EHA(80:20) is shown in *Fig.* 7.6. No significant loss of weight is observed at 230°C. This suggests that the exothermic may be caused by rest curing initiated by unreacted Irgacure 184 or trapped radicals in the network.
The TGA-data are summarised in Table 7.3 as the temperature for different percentages loss of weight (***low***). The TGA experiments show a smooth thermal decomposition of all the acrylate network samples: the samples decompose totally at ± 400°C (no residue left). This suggests that the decomposition of the different acrylate networks follows one main thermal degradation route with the formation of "low" molecular weight (volatile) molecules.

7.3.2. Pyrolysis-MS of cross-linked acrylates

In order to study the network structure of cross-linked acrylates, Pyr-EI-MS was performed. The total ion current (TIC) pyrogram obtained from direct Pyr-EI-MS of cross-linked PEGDA/EHA(80:20) is given in *Fig.* 7.7. In general, one main degradation maximum for each cross-linked PEGDA/EHA network is observed in the pyrogram at a temperature around 400°C. A small fraction at the start (low temperarture) of the temperature resolved pyrogram is observed.

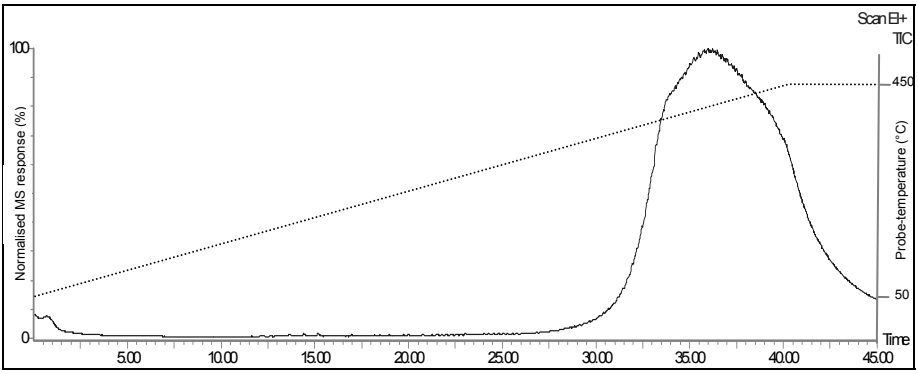

Fig. 7.7. TIC pyrogram of cross-linked PEGDA/EHA(80:20).

A typical MS-spectrum of the main fraction at ± 400°C of PEGDA/EHA(80:20) is given in *Fig.* 7.8. The MS-spectrum shows intense fragment ion series of *m/z* = 45, 89, 133, 177, …, 397. These fragment ions are indicative for PEG ($[H\text{-}(\text{-}O\text{-}CH_2\text{-}CH_2)_n]^+$). The observed ion peak intensities for these PEG related products are maximal at *m/z* 45, while the average M_n of the PEG is 558 *Da* [12].

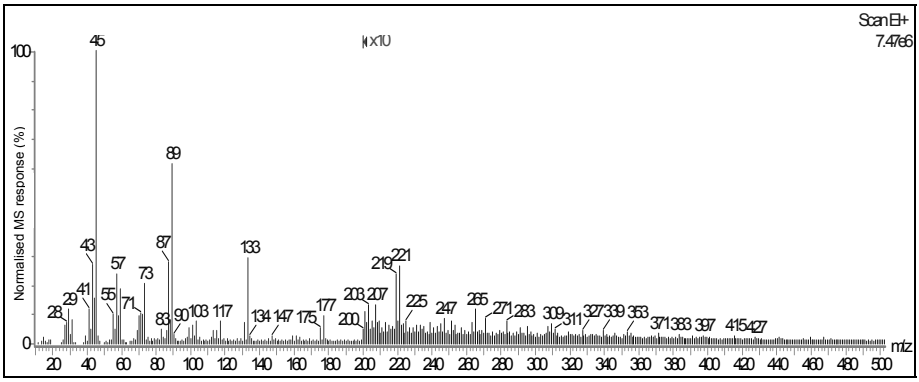

Fig. 7.8. EI-MS-spectrum of main fraction at ± 400°C of cross-linked PEGDA/EHA(80:20).

Table 7.4. The observed fragment ions PEGDA/EHA(80:20) as observed by Pyr-EI-MS

Series	Fragment ions (*m/z*)	Structure proposals
P1	31	$HO\text{-}CH_2^+$
	45	$[H\text{-}(\text{-}CH_2\text{-}CH_2\text{-}O)]^+$
	89, 133, .., 353	$[H\text{-}(\text{-}CH_2\text{-}CH_2\text{-}O)_n]^+$
P2	43	CH_3CO^+ as $[O{=}CH\text{-}CH_2]^+$
	87	$[O{=}CH\text{-}CH_2\text{-}O\text{-}CH_2\text{-}CH_2]^+$
	131, 175, .., 263	$[O{=}CH\text{-}CH_2\text{-}(\text{-}O\text{-}CH_2\text{-}CH_2)_n]^+$
E1	57	$C_4H_9^+$
	70	$C_5H_{10}^{+\bullet}$
	98	$C_7H_{14}^{+\bullet}$
	112	$C(\text{-}C_4H_9)(C_2H_5)(=CH_2)^{+\bullet}$
A1	29	HCO^+
	55	$[H_2C{=}CH\text{-}CO]^+$
	99	$[H_2C{=}CH\text{-}CO\text{-}O\text{-}CH_2\text{-}CH_2]^+$
A2	71	$[H_2C{=}CH\text{-}CO\text{-}O]^+$
	115	$[H_2C{=}CH\text{-}CO\text{-}O\text{-}CH_2\text{-}CH_2\text{-}O]^+$
A3	73	$[H_3C\text{-}CH_2\text{-}CO\text{-}O]^+$
	117	$[H_3C\text{-}CH_2\text{-}CO\text{-}O\text{-}CH_2\text{-}CH_2\text{-}O]^+$
A4	57	$[H_3C\text{-}CH_2\text{-}CO]^+$

	101	$[H_3C\text{-}CH_2\text{-}CO\text{-}O\text{-}CH_2\text{-}CH_2]^+$
I1	81	$C_6H_9^+$
	99	$C_6H_{10}OH^+$
	105	$C_6H_5CO^+$

Beside this main series, other fragment ion series are observed and are assigned as summarised in Table 7.4. Two series reflecting the PEG chains between network junctions were observed (Table 7.4, *P1* and *P2*). In addition, four series at lower abundance were observed (Table 7.4, *A1-A4*). These fragment ions are formed by backbone chain scissions reactions, yielding an acrylate fragment (Table 7.4, *A1* and *A2*) or a hydrogenated acrylate fragment (Table 7.4, *A3* and *A4*). To explain the formation of these ions (*A1-A4*), the polyacrylate backbone chain has to be thermally broken (depolymerisation of the main backbone chain).

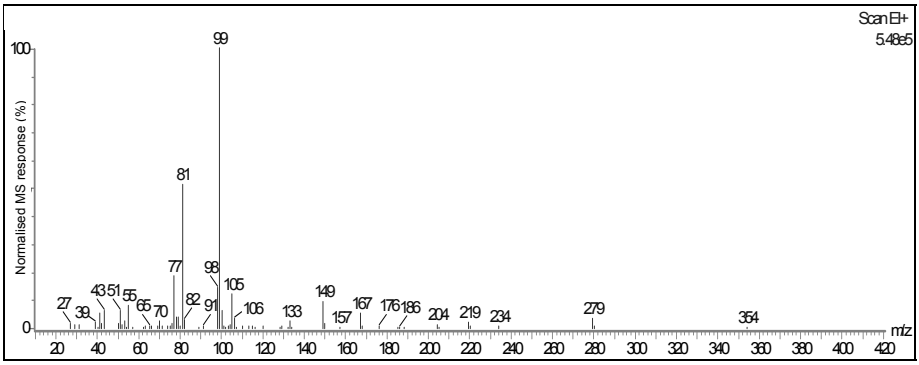

Fig. 7.9. EI-MS-spectrum of the fraction at low temperature of cross-linked PEGDA/EHA(80:20).

The fragment ions *E1* originate from 2-ethyl-1-hexyl acrylate. The *m/z* reconstructed pyrograms of the 2-ethyl-1-hexyl acrylate fragment ions (not shown) show the presence of these ions in the main fraction around 400°C. This indicates the presence of reacted EHA in the sample.

Beside EHA and PEGDA, the coating contains about 1% (*w/w*) Irgacure 184 (M_w = 204 *Da*). The MS-spectrum of the fraction at low temperature is given in *Fig.* 7.9, which show the characteristic fragment ions of Irgacure 184; *m/z* = 81 ($C_6H_9^+$), 99 ($C_6H_{10}OH^+$) and 105 ($C_6H_5CO^+$). The *m/z* reconstructed pyrograms of the Irgacure 184 fragment ions are shown in *Fig.* 710. These *m/z* reconstructed pyrograms show a fraction at low temperature, which can be

explained by unreacted Irgacure 184. The photo-initiator fragments were also observed in the main fraction around 400°C. Since the photo-initiator has the potential to graft onto the polymeric backbone via the hydroxyl-functional group; these fragments are probably related to the reacted grafted photo-initiator.

The observed thermal degradation products after Pyr-EI-MS of UV-cured PEGDA/EHA are characteristic for the network formed; the PEG fragmentation products arise from the chains between the network junctions, while the acrylate related fragments are considered to be formed by unzipping of the polyacrylate backbone chain. From this it can be concluded that the PEGDA/EHA network structure consists of PEG, polyacrylate backbone, EHA and Irgacure 184. However, additional fragmentation upon ionisation at 70 eV makes it difficult to obtain more information about the network structure, such as the chain-length distributions of the chains between network junctions or even error structures (*e.g.* the presence of PEGMA).

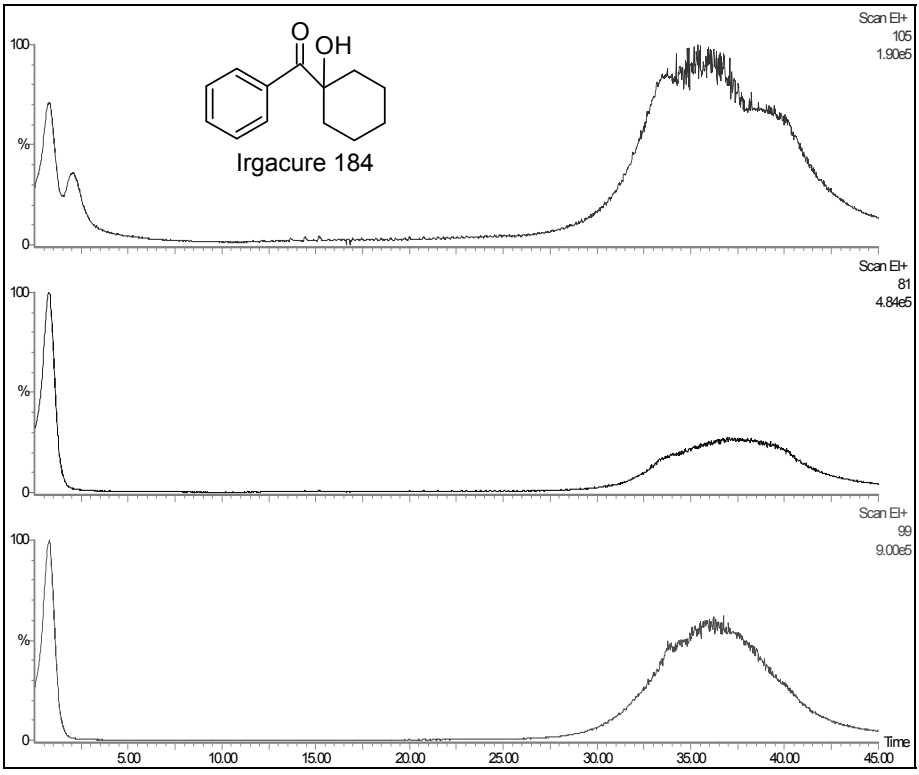

Fig. 7.10. M/z reconstructed pyrograms of the fragments ions of Irgacure 184; m/z = 81 ($C_6H_9^+$), 99 ($C_6H_{10}OH^+$) and 105 ($C_6H_5CO^+$).

As shown, the experiments with probe-EI-MS show relative low-molecular-weight ions, which are fragmented by heating and/or during ionisation. To observe molecular ions reflecting the products formed as result of thermal degradation, the pyrolysis experiments were repeated using probe-CI-MS. The advantage of CI over EI is the production of abundant molecular mass ion peaks. The TIC-pyrograms of three different cross-linked PEGDA/EHA mixtures are given in *Fig.* 7.11. The pyrograms show different ion yield optimums: PEGDA/EHA(60:40) has the optimum around 390°C, while PEGDA/EHA(100:0) has its optimum around 420°C.

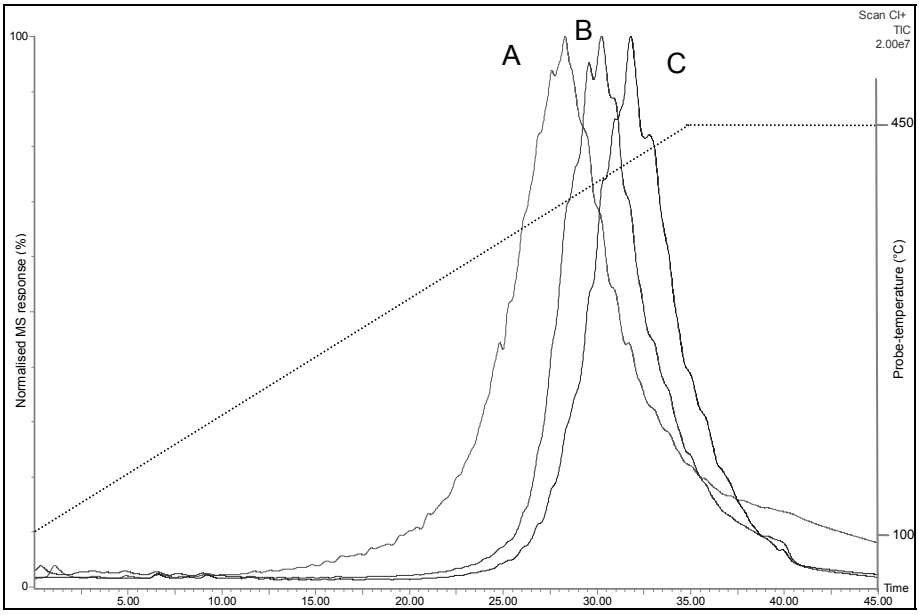

*Fig. 7.11. TIC-pyrograms of PEGDA/EHA(60:40) (**A**), PEGDA/EHA(80:20) (**B**) and PEGDA/EHA(100:0) (**C**).*

The MS-spectra of the main fraction of different cross-linked PEGDA/EHA formulations show a main ion series with *m/z* = 124, 168, 212, …, 740 (see *Fig.* 7.12). Since the ions are NH_4^+ cationised, this series has an endgroup of 18 *Da*, with a repeating unit of 44 *Da*. This series is assigned as PEG (HO-$(CH_2$-CH_2-$O)_n$-H). Besides this PEG series, different other PEG-related series are observed, as outlined in Table 7.5. Series *I-VI* reflect the PEG chain between network junctions. These series are considered to be formed by cleavage of C-O and C-C bonds along the PEG chains, resulting in hydroxyl-, ethyl-, methyl-, vinyl-endgroups and combinations of it.

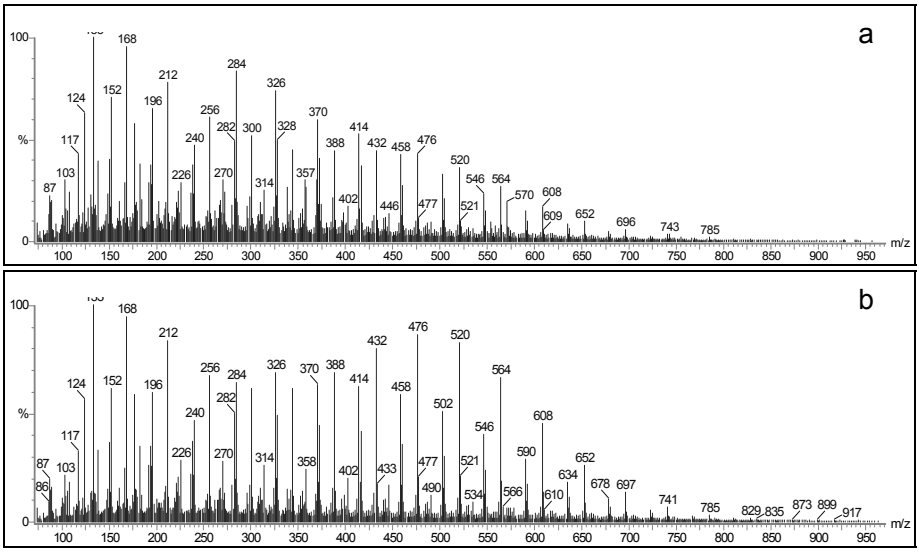

*Fig. 7.12. CI-MS-spectra of the main fraction of the PEGDA/EHA(60:40) (**a**) and PEGDA/EHA(100:0) (**b**).*

Table 7.5. The main NH_4^+ cationised ion series of PEGDA/EHA(80:20) as studied by Pyr-CI-MS

Series	Fragment ions (*m/z*)	Structure proposals
I	124, 168, .., 740	$[HO\text{-}(\text{-}CH_2\text{-}CH_2\text{-}O)_n\text{-}H + NH_4]^+$
II	150, 194,…, 678	$[HO\text{-}(\text{-}CH_2\text{-}CH_2\text{-}O)_n\text{-}CH{=}CH_2 + NH_4]^+$
III	284, 328, …, 548	$[HO\text{-}(\text{-}CH_2\text{-}CH_2\text{-}O)_n\text{-}\ CH_2\text{-}CH_3 + NH_4]^+$
IV	270, 314,…, 534	$[CH_3\text{-}O\text{-}(CH_2\text{-}CH_2\text{-}O)_n\text{-}H + NH_4]^+$
V	210, 254, …,518	$[CH_3\text{-}CH_2\text{-}O\text{-}(CH_2\text{-}CH_2\text{-}O)_n\text{-}CH_3{+}NH_4]^+$
VI	264, 308,…, 484	$[H_2C{=}CH\text{-}O\text{-}(CH_2\text{-}CH\text{-}O)_n\text{-}CH{=}CH_2{+}\ NH_4]^+$
IX	222, 266, …, 662	$[H_2C{=}CH\text{-}CO\text{-}O\text{-}(CH_2\text{-}CH_2\text{-}O)_n\text{-}H + NH_4]^+$

In the temperature-resolved pyrograms of the different samples, series *I* and *II* were observed as the main products. The MS-abundance of the PEG series in the different samples is shown in *Fig.* 7.13. As expected, the observed number-average molecular weight of PEG is higher than that of the PEG distribution as observed by Pyr-EI-MS experiments and is in the M_n range of 558 *Da*, as determined by LC-MS [12]. However, the PEG series originating from PEGDA/EHA(60:40) has a lower molecular weight distribution than the PEG series originating from PEGDA/EHA(100:0), while the molecular weight distribution of PEG in all the samples should be similar. Secondly, the observed

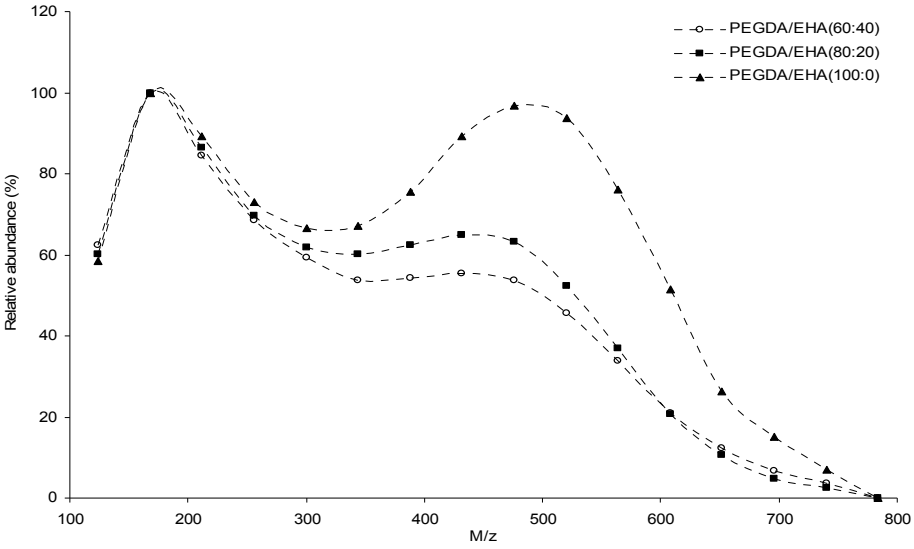

Fig. 7.13. The abundance of [(HO-(CH_2-CH_2-O)$_n$-H)+NH_4^+] ions, as observed in the different acrylate samples as results of Pyr-CI-MS.

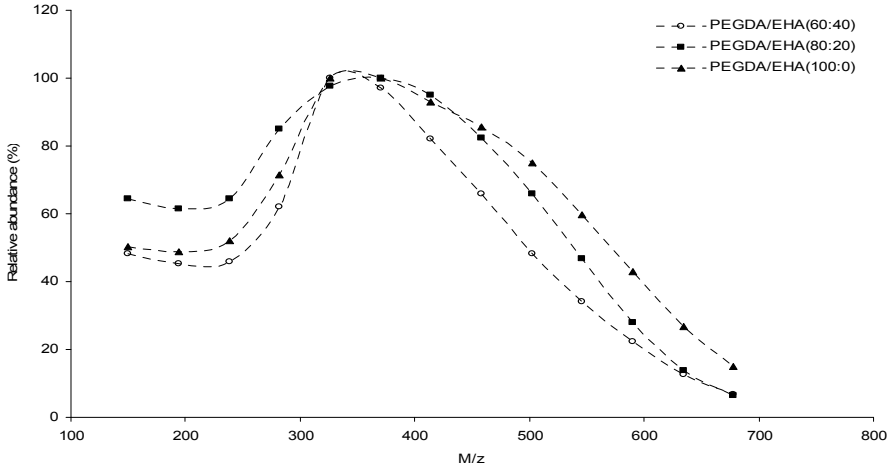

Fig. 7.14. The abundance of [(HO-(CH_2-CH_2-O)$_n$-CH=CH_2)+NH_4^+] ions, as observed in the different acrylate samples as results of Pyr-CI-MS.

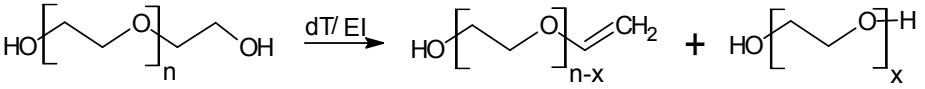

Fig. 7.15. Breakdown of PEG series (dT = energy delivered by heat, EI = energy delivered by ionisation).

distribution is a bimodal distribution (two maxima). These effects are not related to temperature; the MS-spectrum in the front of the main fraction is similar to the MS-spectrum at the back of the main fraction. The ion-abundance of the other main PEG series *II* (HO-(-CH_2-CH_2-O)$_n$-CH=CH_2) for the different samples is shown in *Fig.* 7.14. The average molecular weight of this series is systemically lower compared to series *I*. These observations indicate breakdown of the higher molecular weight PEG series into two lower molecular weight series, as a result of thermal degradation (pyrolysis) and/or fragmentation upon ionisation (see *Fig.* 7.15).
Beside these PEG related products, the series *IX* reflecting polyethylene glycol acrylate oligomers arising from the breakdown of the polyacrylate backbone chain is seen: H_2C=CH-CO-O-(CH_2-CH_2-O)$_n$-H. No indication was found for other ion peaks reflecting the polyacrylate backbone chain, such as polyacrylic acid, polyethene, polypropanal or combinations of it.
The MS-spectra contain at very low abundance other fragments ion series with a odd mass (*m/z* = 87, 103, 107, 117, 133, 161, 177, *etc.*). These fragment ions are protonated ($[M+H]^+$) and can be assigned to the series *I*-*IX*.
The presence of EHA (2-ethyl-1-hexyl acrylate, M_w = 184 *Da*) was investigated by reconstructions of *m/z* ion = 202 ($[M+NH_4]^+$). PEGDA/EHA(60:40) has an intense signal of *m/z* = 202 in the main fraction, opposite to PEGDA/EHA(100:0) (not shown). The absence of *m/z* = 202 in the cross-linked PEGDA/EHA (100:0) makes it likely that this ion is representative for EHA.
The MS-spectrum of PEGDA/EHA(60:40) contains additional ion peaks compared to the MS-spectrum of PEGDA/EHA(100:0): *m/z* = 374 $[M+NH_4]^+$ and *m/z* = 570 $[M+NH_4]^+$. These additional fragments could not be assigned based on the available information and experiments performed.

7.3.3. MALDI-TOF-MS of cross-linked acrylates

The cross-linked PEGDA/EHA networks were investigated by MALDI-TOF-MS. It is well established that the sample preparation protocol influences the sensitivity and selectivity of MALDI-TOF-MS. Many sample preparation techniques have been developed in order to improve the resulting MS-spectrum. The most widely used sampling technique is the “dried droplet method” for the characterisation of soluble polymers [43]. This sample preparation method is very useful for the characterisation of synthetic polymers with narrow polydispersities, since broadly polydisperse polymers show mass discrimination [44]. Solubility of the polymer and miscibility of the polymer with the matrix are important for a representative MS-spectrum [45]. Marie *et al.* demonstrated

the successful use of solvent-free sample preparation methods for the characterisation of PEG [41]. However, still matrix molecules are deposited onto the sample using different deposition methods. Since the cross-linked acrylates are not soluble in any solvent, two uncommon sample preparation methods are used: with and without deposition of different matrix/solvent mixtures at unground, crude ground and fine ground cross-linked acrylate film (see also experimental section).

The MALDI-TOF-MS spectra of the fine ground sample with the different matrices (combinations DHB, Dith, ACN, THF, NaAc at different ratios (1:1, 1:10, 1:100)) show no difference in observed ion peaks, higher than *m/z* = 350. The MS-spectrum in the *m/z* range of 50-350, is different for the different combinations of solvents (ACN, THF) and matrix molecules (Dith, DHB) used. This is probably related to ionisation, fragmentation, recombination and other reactions of the used solvents and matrix molecules. Only at increased laser energies, the MS-spectrum contains clusters of ions around *m/z* = 934.4, *m/z* = 668.6 and *m/z* = 402.8, respectively. These ion clusters do not contain any indication that they are related to PEG or acrylate fragments, which makes it likely that these ion clusters originate from a reaction during or directly after the high-energetic ionisation by MALDI-TOF-MS.

MALDI-TOF-MS analysis of the crude ground PEGDA/EHA(80:20) mixed with Dith and ACN show some low abundance ion peaks, which could be assigned to PEG series. The deposition of different matrix/solvent combinations (combinations DHB, Dith, ACN, THF, NaAc at different ratios (1:1, 1:10, 1:100)) show no difference in observed ion peaks at *m/z* = 350-1500. However, the MALDI-TOF spectrum of the unground PEGDA/EHA(80:20) without any deposition of matrix/solvent and at very high laser energies, shows highly abundant oligomeric fragment ion peaks (see *Figs.* 7.16a and 7.16b). In total, five different series could be observed in the MS-spectrum of the unground PEGDA/EHA(80:20), as outlined in Table 7.6.

Table 7.6. The ion series of PEGDA/EHA(80:20) as observed by MALDI-TOF-MS

Series	Fragment ions (*m/z*)	Structure proposals
I	437.5, 481.5, .., 921.0	$[HO\text{-}(\text{-}CH_2\text{-}CH_2\text{-}O)_n\text{-}H + Na]^+$
I'	497.5, 541.4,…937.0	$[HO\text{-}(\text{-}CH_2\text{-}CH_2\text{-}O)_n\text{-}H + K]^+$
III	553.3, 597.3, …, 817.1	$[HO\text{-}(\text{-}CH_2\text{-}CH_2\text{-}O)_n\text{-}\ CH_2\text{-}CH_3 + Na]^+$
IX	535.5, 579.5, …, 844.2	$[H_2C{=}CH\text{-}CO\text{-}O\text{-}(CH_2\text{-}CH_2\text{-}O)_n\text{-}H + Na]^+$
IX'	551.4, 595.4,…, 815.2	$[H_2C{=}CH\text{-}CO\text{-}O\text{-}(CH_2\text{-}CH_2\text{-}O)_n\text{-}H + K]^+$

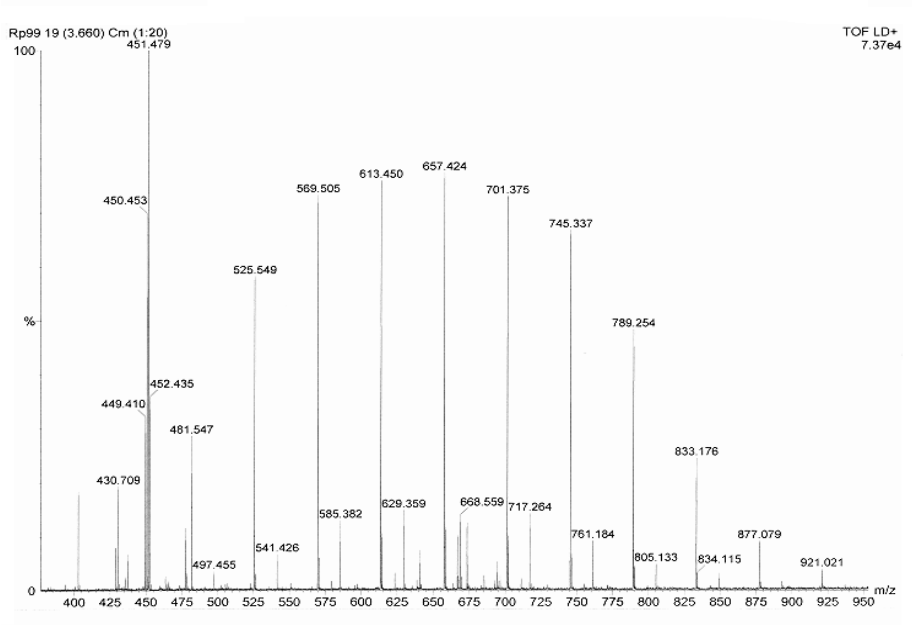

Fig 7.16a. MALDI-TOF-MS spectrum of the unground PEGDA/EHA(80:20) without matrix/solvent addition.

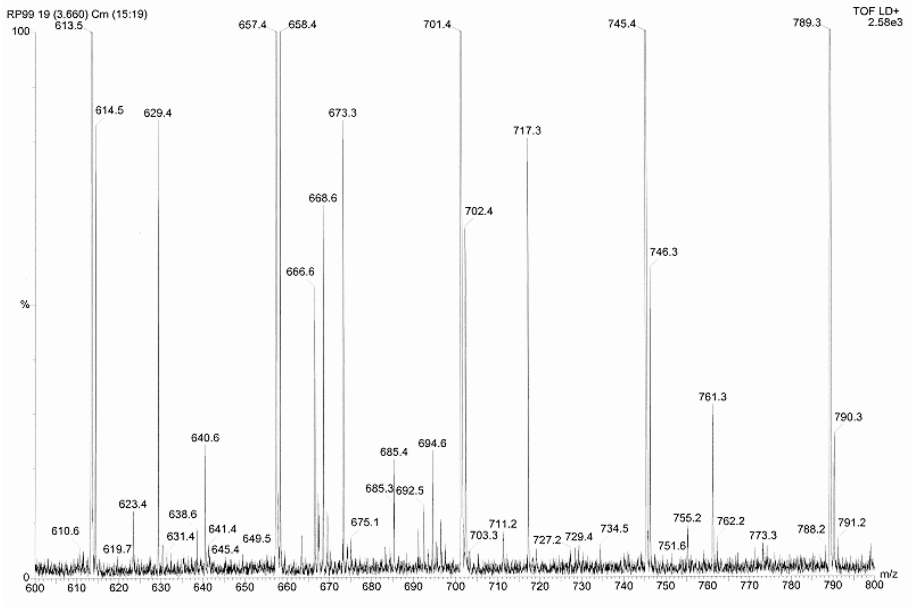

Fig 7.16b. Enlarged MALDI-TOF-MS spectrum (m/z = 600-800) of the unground PEGDA/EHA(80:20) without matrix/solvent addition.

MALDI-ionisation gives mostly single-charged molecular ions [46,47]. Since no mass difference of 22 *Da* is observed between the different oligomeric ion series, it is not possible to make a difference between proton- ($[M+H]^+$) and sodium-cationised ions ($[M+Na]^+$). However, the most abundance series *I* and *I'* show differences of 16 *Da*, which indicates the presence of potassium-cationised ions. The same is true for series *IX* and *IX'*. On the other hand, the mass delta of 16 *Da* can also indicate the presence of additional oxygen in these ions. However, assuming only sodium-cationised ion series, no assignment could be made for one of the most abundance series with *m/z* 497.5±n×44 (endgroup is 34 *Da*). Secondly, the observed abundance of the different oligomeric ion series, fit with the expected abundance of sodium- and potassium-cationised PEG series, *i.e.* the abundance of potassium-cationised PEG series is few orders lower compared to sodium-cationised PEG series [41,46]. Based on this information and the fact that each polymer has a repetitive unit of 44 *Da*, which is the repeating unit of PEG ($–CH_2\text{-}CH_2\text{-}O–$), the different ion series are assigned as outlined in Table 7.6.

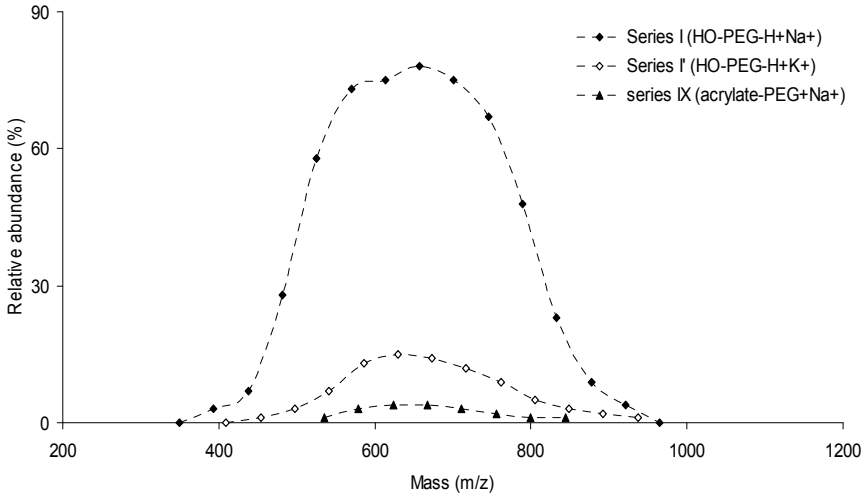

Fig. 7.17. The abundance of the different ion series of PEGDA/EHA(80:20) as observed by MALDI-TOF-MS.

In general, the most abundance series is PEG. Series *IX*, reflecting polyethylene glycol acrylate oligomers arising from the depolymerisation of the polyacrylate backbone chain, was observed in lower abundance. The abundance of both series is given in *Fig.* 7.17. Both series (*I* and *IX*) indicate a similar molecular weight distribution as expected from LC-MS experiments of the starting

material and the hydrolysate [12]. Although the molecular weight distribution of PEG is as expected, possible side reactions [34], degradation [39] and mass discrimination [48] of PEG related compounds, indicate that the MALDI-TOF-MS spectrum has to be quantitatively interpreted with care.
The ion series observed are similar as the main series determined using Pyr-CI-MS. This indicates that the C-O and C-C bonds of the PEG chain between the network junctions and the polyacrylate backbone chains (depolymerisation) are thermally degraded by the laser energy. The molecular weight distribution of PEG, observed by MALDI-TOF-MS is higher (600-700 *Da*) compared to result obtained by Pyr-CI-MS (± 500 *Da*). This can be caused by additional breakdown of the higher molecular weight PEG series into two lower molecular weight series as a result of thermal degradation (pyrolysis) and/or fragmentation upon chemical-ionisation, although mass discrimination of the low-molecular-weight PEG by MALDI-TOF-MS cannot be excluded.
The PEG and PEG-acrylate series determined by direct MALDI-TOF-MS analysis, reflecting the main acrylate network structure. However, no indication was found for the presence of 2-ethyl-1-hexyl acrylate and/or photo-initiator used. Still the fact that fragments ions as result of thermal degradation are observed by direct MALDI-TOF-MS analysis is interesting. Moreover, the MALDI-TOF-MS analyses support the expected network structure of acrylates.

7.3.4. Pyr-LC-MS of cross-linked acrylates

7.3.4.1. Off-line Pyr-LC-MS

To investigate the possibilities of Pyr-LC-MS analysis with respect to unambiguous interpretation of the thermal product fragments of highly cross-linked acrylates, some off-line Pyr-LC-MS experiments were performed. The cross-linked acrylates are pyrolysed using different pyrolysis conditions (see Table 7.1); the samples pyrolysed at 300°C could not be dissolved totally in THF in contrast to the samples pyrolysed at 350-400°C, which are totally soluble in THF. The insoluble thermal residue after heating at 400°C for 277 seconds was deep yellow/brown.
A typical ESI(+)-TIC chromatogram of the PEGDA/EHA(80:20) pyrolysate (Table 7.1, 400°C for 277 seconds), dissolved in THF, is shown in *Fig.* 7.18. Similar, but less intense, TIC-MS chromatograms of cross-linked acrylates, heated at 350°C for 280-880 seconds, were observed. The different compounds are investigated by evaluating their ESI(+)-MS spectra.

Table 7.7. The main ion series of PEGDA/EHA(80:20) as observed by off-line Pyr-LC-MS

Series	t_R (min)	Fragment ions (*m/z*)	Structure proposals
I	18-28	305.1+n×44	$[HO\text{-}(\text{-}CH_2\text{-}CH_2\text{-}O)_n\text{-}H + Na]^+$
II	18-28	287.2+n×44	$[HO\text{-}(\text{-}CH_2\text{-}CH_2\text{-}O)_n\text{-}CH{=}CH_2 + Na]^+$
III	18-28	289.2+n×44	$[HO\text{-}(\text{-}CH_2\text{-}CH_2\text{-}O)_n\text{-}\ CH_2\text{-}CH_3 + Na]^+$
IV	18-28	275.2+n×44	$[CH_3\text{-}O\text{-}(CH_2\text{-}CH_2\text{-}O)_n\text{-}H + Na]^+$
V	18-28	303.2+n×44	$[CH_3\text{-}CH_2\text{-}O\text{-}(CH_2\text{-}CH_2\text{-}O)_n\text{-}CH_3{+}Na]^+$
VI	30	357.2+n×44	$[H_2C{=}CH\text{-}O\text{-}(CH_2\text{-}CH\text{-}O)_n\text{-}CH{=}CH_2{+}\ Na]^+$
VII	29-30	273.1+n×44	$[CH_3\text{-}CH_2\text{-}O\text{-}(CH_2\text{-}CH_2\text{-}O)_n\text{-}CH_2\text{-}CH_3 + Na]^+$
VIII	34-35	345.2+n×44	$[CH_3\text{-}O\text{-}(\text{-}CH_2\text{-}CH_2\text{-}O)_n\text{-}CH{=}CH_2 + Na]^+$
IX	32	359.2+n×44	$[H_2C{=}CH\text{-}CO\text{-}O\text{-}(CH_2\text{-}CH_2\text{-}O)_n\text{-}H + Na]^+$

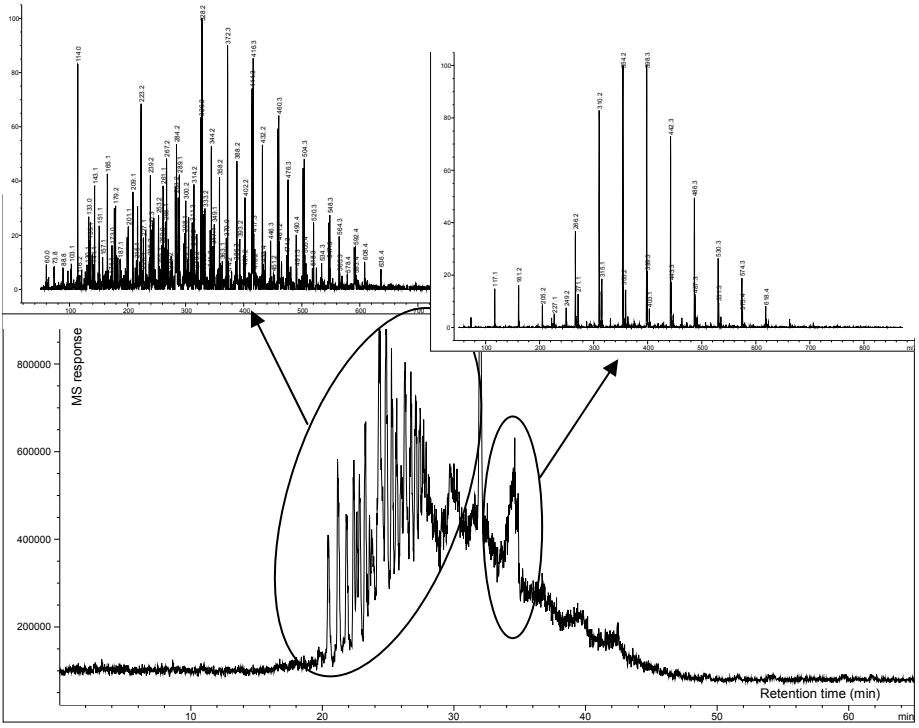

Fig. 7.18. LC-ESI(+)-MS chromatogram of PEGDA/EHA(80:20) pyrolysate, dissolved in THF. Inserted are extracted MS-spectra representing some oligomers series at different eluting times. See experimental section for conditions used.

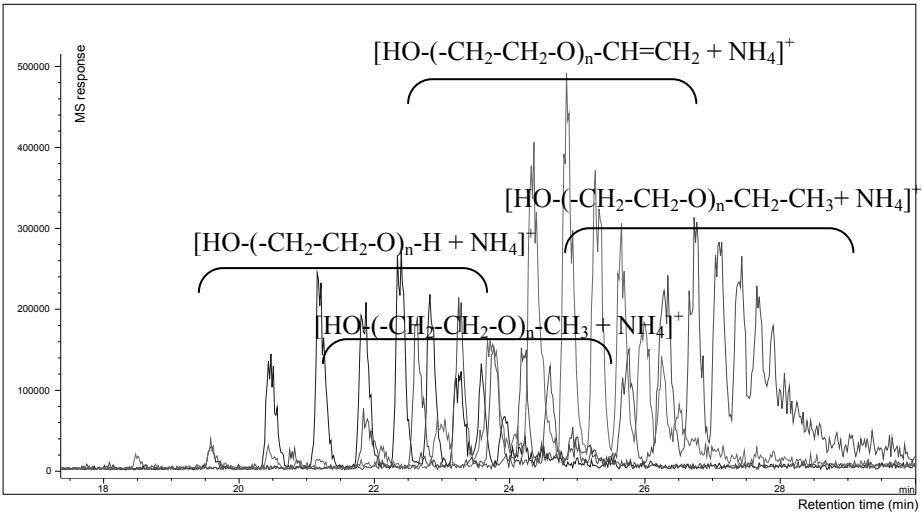

Fig. 7.19. Mass-summarised MS-chromatogram, representing different PEG series.

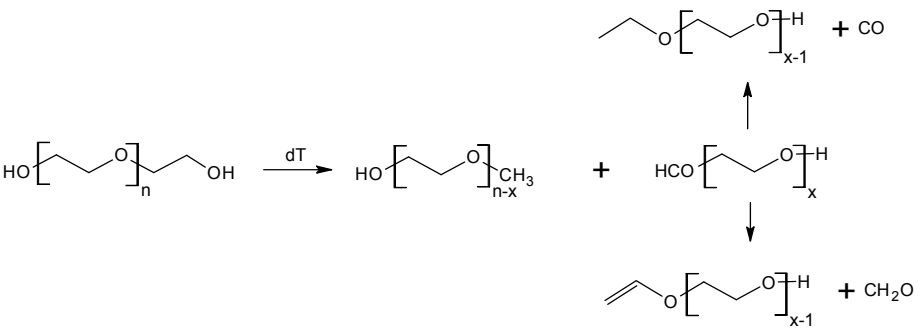

Fig. 7.20. Formation of the different PEG endgroups during the thermal degradation by breaking of the C-C bond (dT = energy delivered by heat).

The low-molecular-weight oligomers could be easily identified by their ESI(+)-MS spectra. Typical ion series with a delta of 44 *Da* are observed, which is the repeating unit of PEG (-CH_2-CH_2-O-). For each oligomeric compound different cationised ions are observed *e.g.* a series of *m/z* = 283.2, 300.2, 305.1 and 321.1, which are singly protonated (isotopic pattern of charge state M+1) ions cationised by proton, ammonia, sodium and potassium, respectively. The ions *m/z* = 283.2, 300.3, 305.1 and 321.1, which have the same retention time (t_R), are identified as HO-(-CH_2-CH_2-O)$_6$-H.

The different oligomeric ion series are assigned as outlined in Table 7.7. At least 9 different PEG containing oligomeric series are observed. It must be pointed

out that the assignment is based on the mass of the endgroup. In some case, more than one structure could fit to the determined endgroups, *e.g. m/z* = 357.2 indicates an endgroup of 26 or 70 *Da*, which could be H_2C=CH-O-(CH_2-CH-O)$_n$-CH=CH_2 or H_2C=CH-CO-O-(CH_2-CH_2-O)$_n$-CH_2-CH=O.
The mass-reconstructed chromatogram of the main PEG series, is shown in *Fig.* 7.19. In general, the series *I-VIII* are caused during the thermal degradation by chain scission of the PEG chains between the chemical network junctions. The main degradation reaction is cleavage of the C-O bond, resulting in a hydroxyl-endgroup and a vinyl-endgroup. This process can be explained by the ionic pathway [49], where hydrogen-transfer of the CH-group is involved (see *Fig.* 7.15). The ethyl-, methyl- but also the vinyl-endgroups can be explained by the thermal degradation of the C-C bond next to the ether-function. The breaking of this bond gives a methyl-endgroup and an unstable product, which will decompose into stable compounds (ethyl- or vinyl-endgroups). The proposed reaction is outlined in *Fig.* 7.20.
The series *IX* originates from the polyacrylate backbone chain, which are caused by the so-called random main-chain scission.

7.3.4.2. On-line Pyr-LC-MS

Thermal degradation studies of cross-linked PEGDA/EHA formulations show that LC-MS analysis of the decomposition products (pyrolysate) of cured acrylates improves the interpretation of the thermal fragments. The use of on-line Curie-Point-Pyr-LC-MS for study of the thermal degradation of cross-linked acrylates is outlined in this section. To perform the dissolution of the products, after pyrolysis, in the pyrolyser liner with a minimum pressure drop, followed by LC-analyses, the on-line CP-Pyr-LC system was designed with an indirect injection procedure. The coupling between the pyrolysis unit and the LC-system was performed with a 500 µL loop, which reduces the pressure drop over the glass pyrolyser liner to almost atmospheric pressure (< 2 bar). To assure dissolution of the pyrolysate, THF was used as a solvent. Since injections of high volumes of THF degraded the quality of the LC-separation, on-line diluting with a weaker solvent and injection on the column follows the dissolution.
The schematic representation of the on-line CP-Pyr-LC system is shown in *Fig.* 7.21. In position A, the pyrolyser liner is purged with pure dry N_2-gas and the sample can be pyrolysed, while the column is equilibrated by aqueous mobile phase. At the same time the loop is purged with pure THF at a flow of 0.2 mL/min delivered by an external pump. After pyrolysis of the sample, the pyrolyser liner is switch into the THF flow (position B), and the thermal

degradation products in the liner are dissolved at atmospheric pressure. After filling the loop with the dissolved pyrolysis products, valve I and II are switched to position C. The pyrolyser liner is switched for cleaning and the next pyrolysis/injection, while the loop is placed into the LC-MS system. The dissolved products are injected onto the column, after diluting with a weaker aqueous solvent.

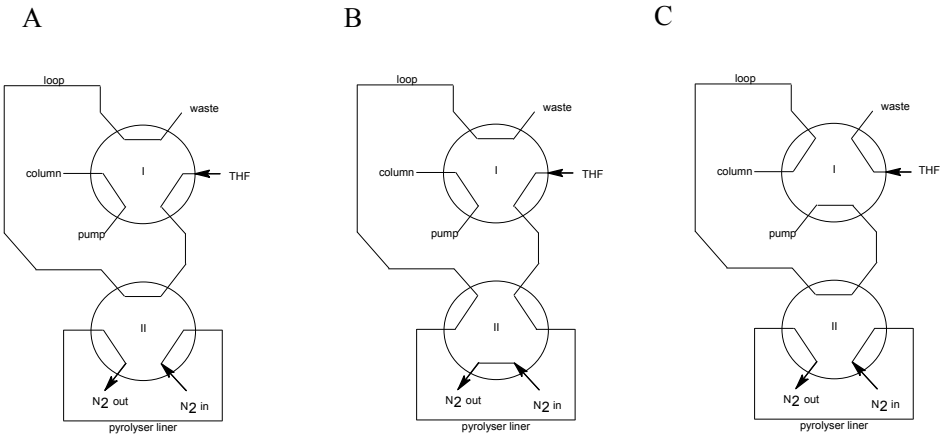

Fig. 7.21. Schematic representation of the CP-Pyr-LC-MS system with "indirect" injection procedure.

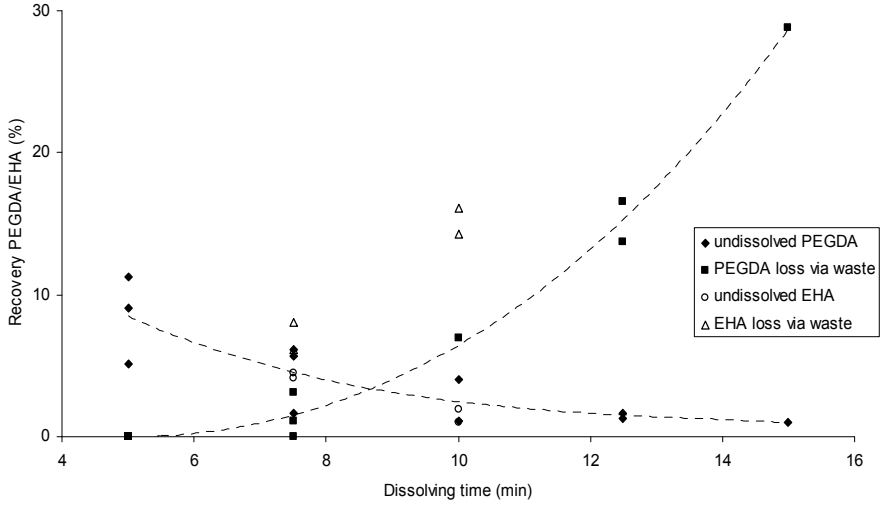

Fig. 7.22. The recovery (% of PEGDA/EHA in CP-liner) versus dissolution time using the indirect injection procedure.

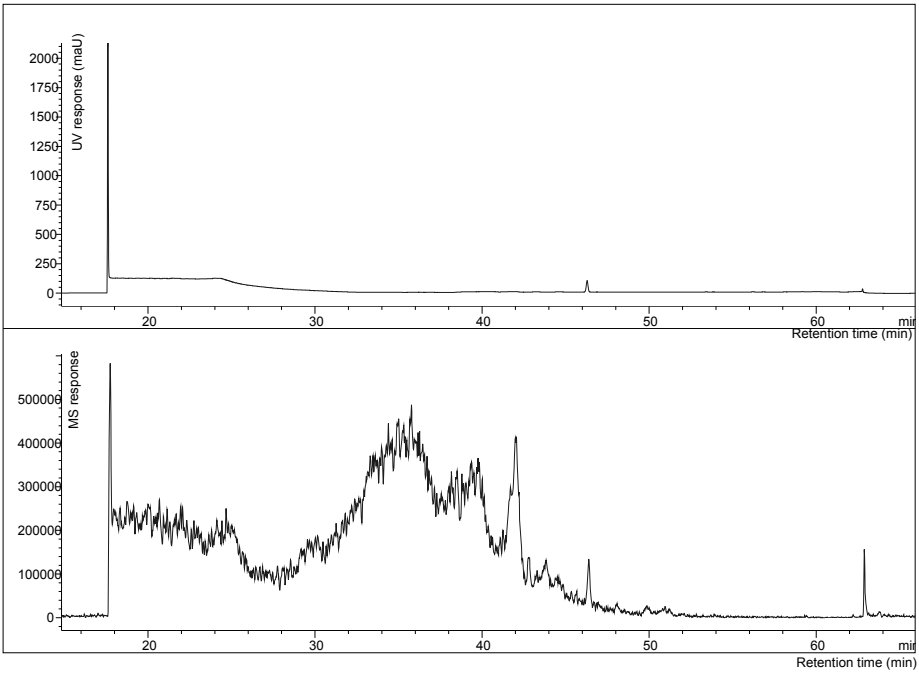

Fig. 7.23. UV- (λ = 210 nm) and TIC-chromatogram of pyrolysed PEGDA/EHA (80:20) at 525°C for 5.0 s.

The dissolution recovery was investigated using PEGDA and EHA as model compounds. Both compounds are placed in the pyrolyser liner and dissolved, injected and analysed using different dissolution times (time position B is 5 min up to 15 min in steps of 2.5 min), flow rates of the THF and concentrations of the model compounds. The recovery (% of PEGDA/EHA in liner) versus dissolution time is shown in *Fig.* 7.22. This graph clearly shows the dissolution process, which is a continuous function of time. For long dissolution times, the compounds are dissolved and are lost via the waste of the loop. For very short dissolution times, the compounds are not totally dissolved and stay behind in the liner. The optimum is around 7.5 min dissolution time under the stated condition for the designed on-line CP-Pyr-LC-MS system. Also at 7.5 minutes a small part of the compounds are not dissolved or get lost via de waste of the loop (<5 % PEGDA and <10 % EHA). The absolute recovery depends on the concentration PEGDA/EHA in the liner; the higher the concentration PEGDA/EHA, the lower the recovery. The flow rate of THF does not significantly influence the recovery. The described experiments show that the on-line CP-Pyr-LC-DAD system, with indirect injection, works well: the model compounds PEGDA and EHA are dissolved and injected for more than 90 % using the stated conditions: 7.5 minutes dissolution time and a flow of 0.2 mL/min THF. The system is not

totally optimised with respect to liner dimensions, liner loop volume, volume damping unit, volume static mixer and other parts, such as liner design (spikes, dead volumes, *etc.*).

On-line pyrolysis experiments of UV-cured PEGDA/EHA were performed with the described on-line CP-Pyr-LC-MS system. Experiments were performed at different pyrolysis temperatures (475, 525, 575, 625, 675 and 800°C) and heating times (5.0 and 9.9 s). A typical UV- and TIC-chromatogram of pyrolysed PEGDA/EHA(80:20) at 525°C for 5.0 s is shown in *Fig.* 7.23.

Table 7.8. The main ion series of PEGDA/EHA(80:20) as observed by on-line pyrolysis-LC-ESI(+)-MS

Series	t_R (min)	Fragment ions (*m/z*)	Structure proposals
I	17-37	305.1+n×44	$[HO\text{-}(\text{-}CH_2\text{-}CH_2\text{-}O)_n\text{-}H + Na]^+$
II	17-37	287.2+n×44	$[HO\text{-}(\text{-}CH_2\text{-}CH_2\text{-}O)_n\text{-}CH{=}CH_2 + Na]^+$
III	17-37	289.2+n×44	$[HO\text{-}(\text{-}CH_2\text{-}CH_2\text{-}O)_n\text{-}\ CH_2\text{-}CH_3 + Na]^+$
IV	17-37	275.2+n×44	$[CH_3\text{-}O\text{-}(CH_2\text{-}CH_2\text{-}O)_n\text{-}H + Na]^+$
V	17-37	303.2+n×44	$[CH_3\text{-}CH_2\text{-}O\text{-}(CH_2\text{-}CH_2\text{-}O)_n\text{-}CH_3{+}Na]^+$
VI	37-42	357.2+n×44	$[H_2C{=}CH\text{-}O\text{-}(CH_2\text{-}CH\text{-}O)_n\text{-}CH{=}CH_2{+}\ Na]^+$
VII	37-42	273.1+n×44	$[CH_3\text{-}CH_2\text{-}O\text{-}(CH_2\text{-}CH_2\text{-}O)_n\text{-}CH_2\text{-}CH_3 + Na]^+$
VIII	37-42	345.2+n×44	$[CH_3\text{-}O\text{-}(\text{-}CH_2\text{-}CH_2\text{-}O)_n\text{-}CH{=}CH_2 + Na]^+$
IX	37-42	359.2+n×44	$[H_2C{=}CH\text{-}CO\text{-}O\text{-}(CH_2\text{-}CH_2\text{-}O)_n\text{-}H + Na]^+$

The different eluted compounds of the pyrolysed UV-cured PEGDA/EHA mixtures (525°C for 5.0 s) are investigated by evaluating their ESI(+)-MS spectra, as described before. The observed and assigned series are outlined in Table 7.8. In general, the same fragment ion series as observed with off-line Pyr-LC-MS were observed.

At t_R = 46.2 min a compound is observed in the UV-chromatogram. This compound has fragment ions of *m/z* = 149.1, 177.1, 223.1 ($[M+H]^+$) and 245.1 ($[M+Na]^+$). This peak is not caused by a blank signal (*e.g.* extraction of the liner septum used *etc.*) and has an UV-maximum of λ = 280 nm. This compound (M_w = 222 *Da*) is probably related to Irgacure 184, but no structure proposal could be made.

The low-molecular-weight oligomers of these series elute as a broad peak from the LC-column. In *Fig.* 7.24, different ion masses of PEG oligomers are reconstructed. These *m/z* reconstructions show that the peak broading is a function of the molecular weight. This is caused by the "low" percentage THF in

the mobile phase, from the dissolution/injection procedure used, which is a too strong eluent for the low-molecular-weight PEG oligomers; THF disrupts the distribution equilibrium between the mobile and stationary phase, which results in band broading. This can probably be avoided by using a weaker eluent during the dissolution/injection procedure by decreasing the percentage THF/weak eluent ratio.

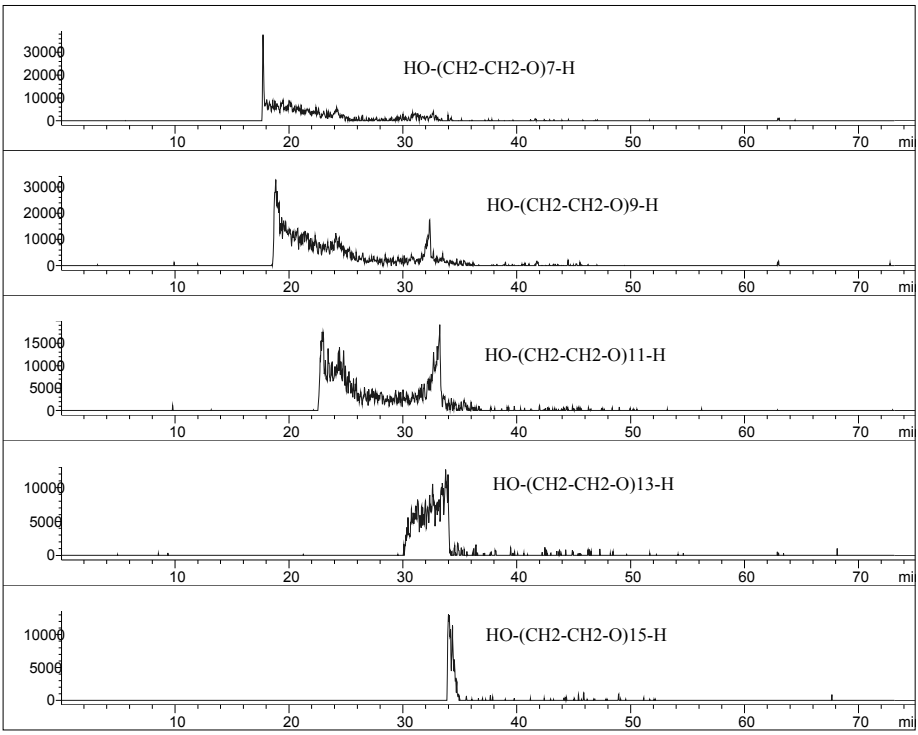

Fig. 7.24. Reconstruction of mass ions of different PEG oligomers ($[PEG+NH_4]^+$).

7.4. Discussion and conclusion

Different thermal degradation methods are used for the characterisation of highly cross-linked non-soluble PEGDA/EHA networks, with different ratios of mono- and bi-functional acrylates.

DSC and TGA analysis give information regarding the thermal decomposition temperature, which decreases with increasing EHA concentrations in the cross-linked PEGDA/EHA mixtures. Secondly, the smooth thermal decomposition observed by TGA suggests one main thermal degradation route of the cross-

linked acrylates with formation of “low” molecular weight fragment molecules. The thermal degradation was studied in more detail using Pyr-EI-MS. These experiments show also one main degradation maximum around 400°C for the different cross-linked PEGDA/EHA networks. The MS-spectra of the different acrylates contain different series reflecting the PEG chains between network junctions and the acrylate backbone chains. Also unreacted and grafted photo-initiator and EHA were observed. Although Pyr-EI-MS gives characteristic fragments, which can be used to characterise the functional groups of the network, no information regarding the molecular weight between network junctions and network imperfections could be observed. The use of Pyr-CI-MS shows the release of higher molecular weight compounds, as the fragmentation upon thermal degradation was minimised. Nevertheless, the ion abundance of different PEG related series indicates breakdown of the higher molecular weight PEG series into two lower molecular weight series. It is unclear if this is the result of thermal degradation or fragmentation upon ionisation or a combination of it.

MALDI-TOF-MS analysis of unground acrylate networks, without matrix/solvent addition, gives similar ion series as determined using Pyr-CI-MS and supports the expected network structure of cross-linked acrylates. No indication was found for the presence of EHA and/or photo-initiator used. Still the fact that fragments ions as result of thermal degradation are observed by direct MALDI-TOF-MS analysis is remarkable.

Off-line Pyr-LC-MS analysis shows different series reflecting the acrylate network structure. The use of LC-MS after pyrolysis helps the interpretation of the thermally produced fragments of these highly cross-linked acrylates. To perform the pyrolysis and LC-MS analysis without additional steps, an on-line Pyr-LC-MS system was designed. The system gives similar results as off-line pyrolysis LC-MS analysis. The on-line Pyr-LC-MS experiments with UV-cured acrylates make rapid screening of various and oligomeric products, which are formed during the pyrolysis, possible. However, peak broading of low-molecular-weight polar compounds, as result of the used dissolution/injection procedure was observed. Additional optimalisation of the used dissolution/injection procedure is needed.

Two main conclusions can be drawn from the different thermal degradation experiments performed.

First, the use of Pyr-MS, MALDI-TOF-MS and Pyr-LC-MS shows the release of thermal degradation fragments which reflect the acrylate network structure, as given in *Fig.* 7.25. The estimated formation of the characteristic products derived from UV-cured PEGDA/EHA by thermal degradation proceeds via two

main steps: scission of the polyacrylate chains and the scission of the PEG chains between network junctions.

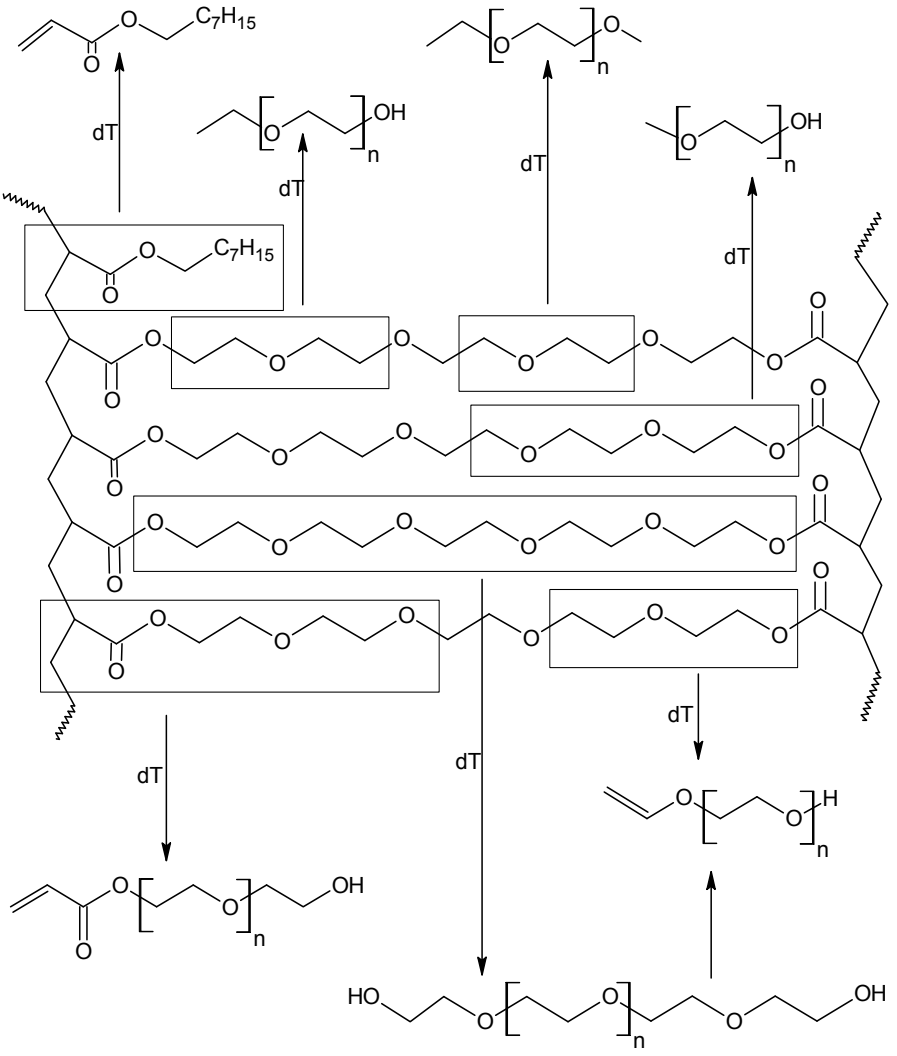

Fig. 7.25. Formation pathway of typical products of PEGDA/EHA by pyrolysis series (dT = energy delivered by heat).

The polyacrylate chains show the formation of polyethylene glycol acrylate oligomers arising from the breakdown of the polyacrylate backbone chain via

the so-called random main-chain scission. The scission depends on the stability of the radicals and the compounds formed. Both the formation of a secondary radical and a C=C bond (the average molar C=C bond enthalpy, which is the energy required to break one mole of bonds between pairs of atoms in the gaseous phase is 611 kJ/mol while the average molar C-C bond enthalpy is 347 kJ/mol) leads to depolymerisation of the polyacrylate backbone chain (see *Fig.* 7.26). The formation of energetically less favourable primary radical leads to acetate or methacrylate evolution, which is not observed in the degradation products using different pyrolysis and analysis methods.
The PEG chains between the network junctions prefer breakdown of the C-O bonds towards hydroxyl- and ethyl-functionalised PEG. Dehydration of the hydroxyl endgroup results in 'vinyl-ether' endgroup. However, the formation of the methyl endgroup indicates cleavage of the C-C bond along the PEG chains as well.

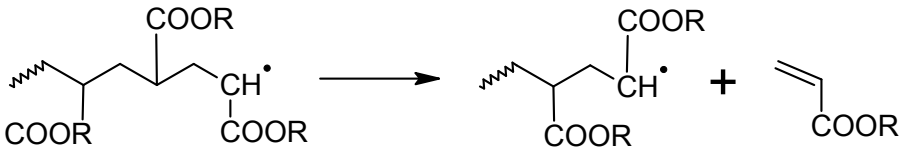

Fig. 7.26. Depolymerisation of the polyacrylate backbone chain.

Secondly, DSC, TGA and Pyr-MS show a changing thermal degradation temperature with the composition of the cross-linked acrylates. The relation between cross-link density, defined as the number-average molecular weight of polymers between cross-links (M_c), and glass-transition temperature (T_g) of a network is well known [50]. The linear relation of the network density, as $1/M_c$, and the T_g for the PEGDA/EHA networks is given in *Fig.* 7.27, which shows the increase of the T_g with increasing network densities.
A linear relation was also observed for the thermal degradation temperature of highly cross-linked acrylate networks and the network density, as shown in *Fig.* 7.28. The thermal degradation temperature determined by Pyr-EI-MS and Pyr-CI-MS show a similar trend, although Pyr-EI-MS shows a higher degradation temperature in contradiction to Pyr-CI-MS analysis. This is probably related to the experimental conditions used (*e.g.* vacuum in the MS-source). The thermal degradation observed with TGA shows a deviating behaviour; the change in degradation temperature is lower compared to Pyr-MS. Both empirical relations with the network density (of T_g or degradation temperature) can be used for a

fast determination of network density.

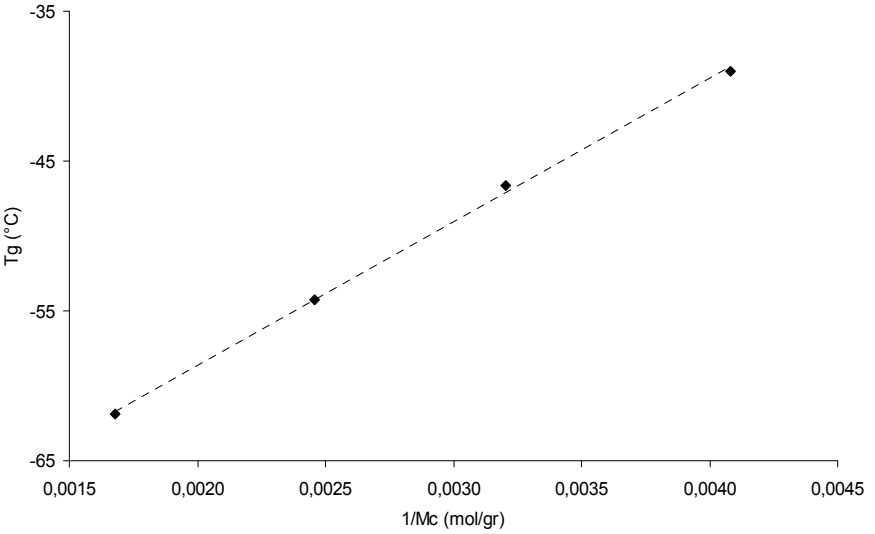

Fig. 7.27. Experimental relation between network density ($1/M_c$) and T_g of highly cross-linked acrylate networks.

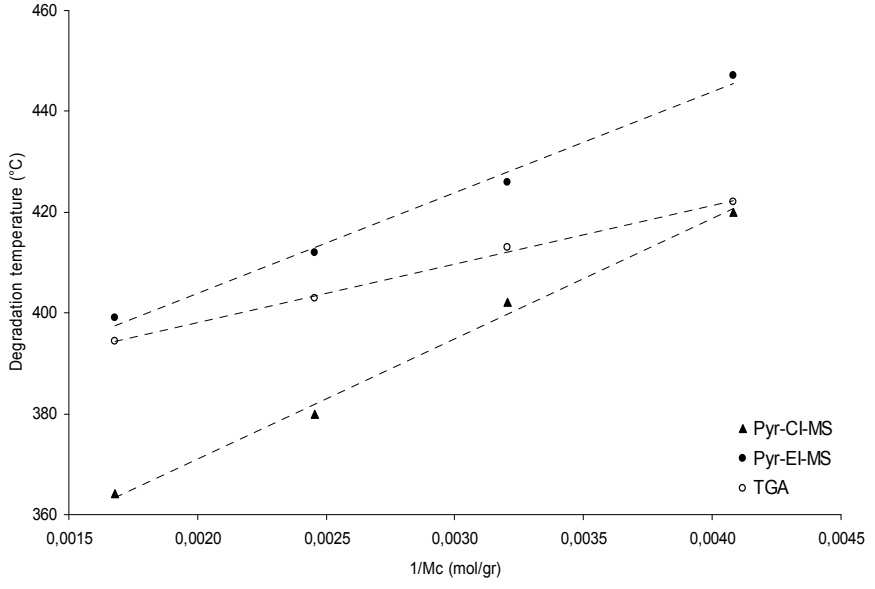

Fig. 7.28. Experimental relation between network density ($1/M_c$) and degradation temperature (TGA and Pyr-MS) of highly cross-linked acrylate networks.

Concluding, thermal degradation methods followed by direct MS or LC-MS analysis, cause thermal degradation products of cross-linked acrylates which give insight in the chemical composition of the PEGDA/EHA network structure. The different thermal degradation reactions, which result in different oligomeric series, make it difficult to translate the results quantitatively to a network structure. However, no indication of network imperfections was observed, which make thermal degradation methods only valid for supporting the anticipated acrylate network structure. Thermal degradation temperatures can be related to the network density, using empirical relations.

References

[1] Resins for coatings, Chemistry, Properties and Applications, Ed. D. Stoye and W. Freitag, Hanser/Gardner Publications, Inc., Cincinnati (1996).

[2] The physics of polymers, Concepts for understanding their structures and behaviour, G.R. Strobl, Springer Verslag Berlin-Heidelberg (1996/1997).

[3] C. Decker, Macromol. Rapid Commun. 23 (2002) 1067.

[4] S.M. Gasper, D.N. Schissel, L.S. Baker, D.L. Smith, R.E. Youngman, L.-M. Wu, S.M. Sonner, R.R. Hancock, C.L. Hogue, S.R. Givens, Macromolecules 39 (2006) 2126.

[5] A.A. Dias, H. Hartwig, J.F.G.A. Jansen, Surf. Coat. Int. 83 (2002) 382.

[6] K.S. Anseth, C. Decker, C.N. Bowman, Macromolecules 28 (1995) 4040.

[7] G.R. Tryson, A.R. Schultz, J. Polym. Sci. 17 (1979) 2059.

[8] G.P. Simon, P.E. Allen, D.J. Bennett, D.R.E. Williams, E.H. Williams, Macromolecules 22 (1989) 3555.

[9] V.M. Litvinov, A.A. Dias, Macromolecules 34 (2001) 4051.

[10] J.A. Burdick, T.M. Lovestead, K.S. Anseth, Biomacromolecules 4 (2003) 149.

[11] A.K. Burkoth, K.S. Anseth, Macromolecules 32 (1999) 1438.

[12] R. Peters, V.M. Litvinov, P. Steeman, A.A. Dias, Y. Mengerink, R. van Benthem, C.G. de Koster, Sj. van der Wal, P. Schoenmakers, J. of Chromatogr. A 1156 (2007) 111.

[13] J.B. Hutchsion, A.S. Lindquist, K.S. Anseth, Macromolecules 37 (2004) 3823.

[14] W.J. Irwin, J. Anal. Appl. Pyrol. 1 (1979) 3.

[15] R.G. Davidson, J. Anal. Appl. Pyrol. 16 (1989) 143.

[16] J.J. Boon, Int. J. Mass Spectrom. Ion Processes 118/119 (1992) 755.

[17] S.C. Moldoveanu, Analytical pyrolysis of natural organic polymers, Elsevier, Amsterdam (1998).

[18] D. Hummel, F. Scholl, Atlas der Polymer- und Kunstoffanalyse, Band 2 Teil b/I, Hanser Verslag, Munchen (1988).
[19] F.C.-Y. Wang, J. Anal. Appl. Pyrol. 71 (2004) 83.
[20] H. Nakagwa, S. Tsuge, K. Murakami, J. Anal. Appl. Pyrol. 10 (1986) 31.
[21] H. Nakagwa, S. Tsuge, Macromolecules 18 (1985) 2068.
[22] J.M. Challinor, J. Anal. Appl. Pyrol. 18 (1991) 233.
[23] K. Oba, Y. Ishida, H. Ohtani, S. Tsuge, Polym. Degrad. Stab. 76 (2002) 85.
[24] H. Matsubara, A. Yoshida, Y. Kondo, S. Tsuge, H. Ohtani, Macromolecules 36 (2003) 4750.
[25] E.R.E. van der Hage, J.J. Boon, J. of Chromatogr. A 736 (1996) 61.
[26] F. Bertini, G. Audisio, V.V. Zuev, Polym. Degrad. Stab. 89 (2005) 233.
[27] G.G. Cameron, D.R. Kane, J. Polym. Sci. 2 (1964) 693.
[28] N. Grassie, D.H. Grant, Polymer 1 (1960) 445.
[29] R.S. Lehrle, E.J. Place, Polym. Degrad. Stab. 56 (1997) 215.
[30] J.P. Mahalik, G. Madras, Ind. Eng. Chem. Res. 44 (2005) 4171.
[31] L. Gunawan, J. K. Haken J. Polym. Sci. 23 (2003) 2539.
[32] M. Milovanovic, R. Boskovic, T. Tosic, L. Katsaikas, I.G. Opovic, Polym. Degrad. Stab. 91 (2006) 3221.
[33] V.V. Zuev, F. Bertini, C. Audisio, Polym. Degrad. Stab. 91 (2006) 512.
[34] N. Grassie, J.G. Speakman, J. Polym. Sci. 9 (1971) 919.
[35] A. Eisenbrug, T. Yokoyama, E. Sambalido, J. Polym. Sci. 7 (1969) 1717.
[36] R.P. Lattimer, J. Anal. Appl. Pyrol. 68-69 (2003) 3.
[37] I.C. McNeill, Thermal analysis, 3, p 27, ed H.G. Wiedeman, Birkhauser Verslag, Basel (1972).
[38] R.P. Lattimer, J. Anal. Appl. Pyrol. 56 (2000) 61.
[39] T.L. Sleby, C. Wesdemioitis, R.O. Lattimer, J. Am. Soc. Mass Spectrom. 5 (1994) 1081.
[40] Analytical Pyrolysis of Synthetic Organic Polymers, Serban Moldoveanu, Elsevier, Amsterdam (2005).
[41] A. Marie, F. Fournier, J.C. Tabet, Anal. Chem. 72 (2000) 5106.
[42] H. Seongok, K. Chongyoup, K. Dongsook, Polymer, 38 (1997) 317.
[43] K. Tanaka, H. Waki, W. Ito, S. Akida, T. Yoshida, T. Yoshida, Rapid, Commun. Mass Spectrom. 2 (1988) 151.
[44] D.C. Schriemer, L. Li, Anal. Chem. 69 (1997) 4169.
[45] C.M. Kassis, J.M. DeSimone, R.W. Linton, G.W. Lange, R.M. Friedman, Rapid Commun. Mass Spectrom. 11 (1997) 1462.
[46] J. H. Scrivens and A.T. Jackson, Int. J. of Mass Spectrom. 200 (2000) 261.
[47] D. Muscat, H. Henderickx, G. Kwakkenbos, R. van Benthem, C.G. de Koster, R. Fokkens, N.N.M Nibbering, J. Am. Soc. Mass Spectrom. 11 (2000) 218.
[48] R.S. Lehrle, D.S. Sarson, Rapid Commun. Mass Spectrom. 9 (1995) 91.

[49] I. Mita, Aspects of degradation and stability of polymers, Elsevier, Amsterdam, (1978) 248.
[50] T.G. Fox, S. Loshaek, J. Polym. Sci. 15/371 (1955) 391.